Supplementary Information and Discussion for "The increasing importance of atmospheric demand for ecosystem water and carbon fluxes"

Contents:

Section S1: Ameriflux Data Quality Control and filtering: Ameriflux Study Sites are described in Table S1:

Table S1: The Ameriflux synthesis sites. 'h' indicates canopy height. The 'DOY start' and 'DOY end" dates indicate the start and end of the site-specific analysis period, which is assumed to be the period of time during which leaf area index is relatively contstant. DI_PM indicates the dryness index (= mean annual potential evapotranspiration/precipitation) determined using the Penman-Monteith model for potential evapotranspiration. 'MAP' is mean annual precipitation derived from the FLUXNET database. Sites that are included in the analysis of future climate effects are indicated with a 'Y.'

SITE NAME	CODE	LAT	LONG	STATE	TYPE	h (m)	Years used	DOY Start	DOY End	DI_PM	MAP (mm)	Future analysis?	Reference
ARM - MAIN	US-ARM	36.61	-97.49	OK	CRO	0.5	2003-2012	141	239	1.52	843	Y	1
Bartlett Experimental Forest	US-BAR	44.06	-71.29	NH	DBF	19	2005-2011	169	225	0.76	1246		2
Black Hills	US-BLK	44.16	-103.65	SD	ENF	12	2004-2008	169	225	2.4	574		
Blogett	US-BLO	38.9	-120.63	CA	ENF	7	2001-2007	170	250	1.08	1226		3
Bondville Main	US-BO1	40.01	-88.29	IL	CRO	3	2001-2008	210	270	1.02	991	Y	4
Brooks Field 11	US-BR3	41.97	-93.69	IA	CRo	1	2005-2011 (odd)	200	250	0.67	847		5
Duke Forest hardwood	US-DK2	35.97	-79.09	NC	DBF	27	2001-2008	141	239	1.24	1170	Y	6,7
Duke Forest loblolly pine	US-DK3	35.98	-79.09	NC	ENF	16.5	2001-2008	127	253	1.37	1170	Y	6,7
Duke Forest open field	US-DK1	35.97	-79.1	NC	GRA	1	2001-2008	141	239	1.18	1170	Y	6,7
Fermi Agriculture	US-IB1	41.86	-88.22	IL	CRO	0.3	2005-2011 (odd)	200	250	0.56	929		8
Fermi Prairie	US-IB2	41.84	-88.24	IL	GRA	0.3	2005-2011	155	225	0.918	930		8
Flagstaff Managed Forest	US-FMF	35.09	-111.763	AZ	ENF	18	2006-2010	169	239	4.02	546		9
Flagstaff Unmanaged Forest	US-FUF	35.09	-111.76	AZ	ENF	18	2006-2010	169	267	3.38	562		9
Freeman Ranch	US-FR2	29.95	-98	TX	SAV	4	2005-2008	113	281	2.15	864		10
GLEES	US-GLE	41.36	-106.24	WY	ENF	12.1	2005-2012	210	240	0.93	525		11
Kansas Field Station	US-KFS	39.06	-95.19	KS	GRA	0.5	2008-2012	140	253	1.02	1014		12
Kendall Grassland	US-WKG	31.74	-109.94	AZ	GRA	0.1	2005-2012	113	281	4.36	407		13
KennedyScrub Oak	US-KS2	28.61	-80.67	FL	SRB	1.5	2000-2006	29	337	0.8	1310		
Konza Prairie	US-KON	39.08	-96.56	KS	GRA	0.4	2007-2012	141	239	1.4	867		12
Lucky Hills Shrubland	US-WHS	31.75	-110.05	AZ	SRB	1	2008-2012	113	281	7.89	320	Y	13
Mary's River Fir	US-MRF	44.65	-123.55	OR	ENF	34	2006-2011	141	253	0.45	1820		14
Mead Irrigated	US-NE1	41.17	-96.48	NE	CRO	1	2001-2012	200	250	0.862	790		15
Mead Rainfed	US-NE3	41.18	-96.44	NE	CRO	1	2001-2011 (odd)	200	250	0.429	784		15
Metolius Intermediate Pine	US-ME2	44.45	-121.56	OR	ENF	22	2002-2012	169	225	2.55	523	Y	16
Metolius Second Young Pine	US-ME3	44.5	-121.62	OR	ENF	3	2004-2007	155	220	1.41	719		17
Missouri Ozark Site	US-MOZ	38.74	-92.2	MO	DBH	24.2	2004-2010	141	239	1.89	986	Y	18,19

Table S1 continued

SITE NAME	CODE	LAT	LONG	STATE	TYPE	h (m)	Years used	PGS Start	PGS End	DI_PM	MAP (mm)	Future analysis?	Reference
Morgan-Monroe State Forest	US-MMS	39.32	-86.41	IN	DBF	27	2000-2012	141	239	1.43	1032	Y	20
NC loblolly pine	US-NC2	35.8	-76.67	NC	ENF	14.1	2005-2010	113	267	1.24	1320		21
Niwot Ridge	US-NR1	40.03	-105.55	CO	ENF	11.5	2000-2012	160	230	1.76	800	Y	22
Oak Openings	US-OHO	41.55	-83.84	OH	DBF	24	2004-2012	160	239	1.2	849	Y	23
Santa Rita Creosote	US-SRC	31.91	-110.84	AZ	SRB	1.7	2008-2012	57	281	5.56	294[*]		24
Santa Rita Grassland	US-SRG	31.79	-110.83	AZ	GRA	0.5	2008-2014	85	267	5.85	420		
Santa Rita Mesquite	US-SRM	31.82	-110.87	AZ	SAV	2.5	2004-2012	71	281	8.06	380	Y	13
Sylvania	US-SYV	46.24	-89.35	MI	ENF	22	2001-2008	169	239	0.8	380	Y	25
Tonzi Ranch	US-TON	38.43	-120.97	CA	SAV	9	2001-2012	100	170	3.48	559	Y	26
U. of MI Biological Station	US-UMB	45.56	-84.71	MI	DBF	21	2007-2012	169	239	1.347	803		27
Vaira Ranch	US-VAR	38.41	-120.95	CA	GRA	0.55	2000-2012	100	170	2.28	559	Y	26
Walker Branch	US-WBW	35.96	-84.29	TN	DBH	25	1998-2006	141	253	0.8	1372	Y	28
Willow Creek	UW-WCR	45.81	-90.08	WI	DBF	24.2	2000-2012	183	225	0.59	787		25

[*] *Mean annual precipitation data were not reported to FLUXDATA.org for this site; MAP is therefore that reported in reference 24*

1 Half-hourly or hourly records of eddy-covariance derived ET and ancillary meteorological data were
2 obtained from 38 Ameriflux sites in the continental U.S. Sites were chosen for inclusion in the study if at
3 least four years of data, including soil moisture data, were available and generally free of large gaps,
4 though most flux records were much longer (see Table S1).

5 *Hourly data quality control*: The ET data were subjected to a standardized quality control procedure
6 whereby data were first filtered to remove missing data and ET measurements greater than 2 mm/hour or
7 less than 0.6 mm/hour. Meteorological data were also screened for obvious outliers (i.e. air temperature
8 less than -30°C or greater than 50°C, VPD < 0, net radiation less than -500 W m^{-2} or greater than 1500 W
9 m^{-2}). Data were not gapfilled; rather, all analysis relied only on screened observations. Most of the
10 analysis was limited to daytime periods ($Rn > 50$ W m^{-2}) when wind speed exceeded 1 m s^{-1} and VPD >
11 0.6 kPa (to minimize stability effects).

12 *Filtering data to periods of relatively stationary leaf area index:* Our analysis includes sites that span a
13 wide range of leaf area index and canopy height, which are variables known to affect vegetative hydraulic
14 functioning[29, 30]. Within a site, temporal variation in leaf area or other aspects of canopy architecture were
15 not explicitly considered, though they may also have affected the temporal dynamics of ET. To minimize
16 the influence of those effects, we filtered our data to exclude periods when leaf area was expected to be
17 low or highly dynamic. In evergreen forests, the analysis period was defined to start two weeks after the
18 average date of the last sub-zero hourly air temperature observation, and was defined to end one week
19 before the average date of the first sub-zero hourly air temperature observation in the fall/winter. In
20 deciduous forests and temperate grasslands, the analysis period was defined to start three weeks after the
21 average date of the last sub-zero hourly air temperature observation, and was defined to end two weeks
22 before the average date of the first sub-zero hourly air temperature observation in the fall/winter. In
23 croplands, semi-arid grassland and shrublands, and Mediterranean ecosystems (i.e. US-TON, US-VAR),
24 the analysis period was defined based on previously published site-specific estimates of leaf area or
25 communication from site data providers. The start and end of the analysis period at each site are given in
26 Table S1.

27 *Limiting the analysis to exclude low* VPD**:** When parameterizing the model of Eq. 1 in the main text, we
28 limited the data to those collected when VPD > 1.0 kPa. This approach is consistent with other work[31],
29 and recognizes that estimates of conductances become unreliable when they are derived by dividing
30 measured water fluxes by near-zero VPD. Furthermore, at low VPD when atmospheric conditions are
31 often stable, boundary layer conductances may become an important constraint on observations of ET.
32 These challenges are exacerbated by the fact that, at low VPD, ET fluxes are also low and of a magnitude
33 comparable to the uncertainty in the observations themselves.

34 When using the soil-moisture-specific parameterizations of Eq. 1 to determine the total growing season
35 limitations to G_S and ET, we assume that VPD is not limiting when it is less than 0.6 kPa. To an extent,
36 this assumption is one of convenience, since the model of Eq. 1 can produce large errors when VPD is
37 close to zero (and ln(VPD) is approaching infinity). We note, however, that the difference between PET
38 and ET is typically near zero or negative when VPD < 0.6 kPa (Figure S1). Specifically, across all sites, a
39 linear model for PET-ET as a function of VPD tends to cross zero at VPD = 0.6 kPa on average (std.dev =
40 0.3 kPa), indicating that at low VPD, ET is not limited from its potential rate.
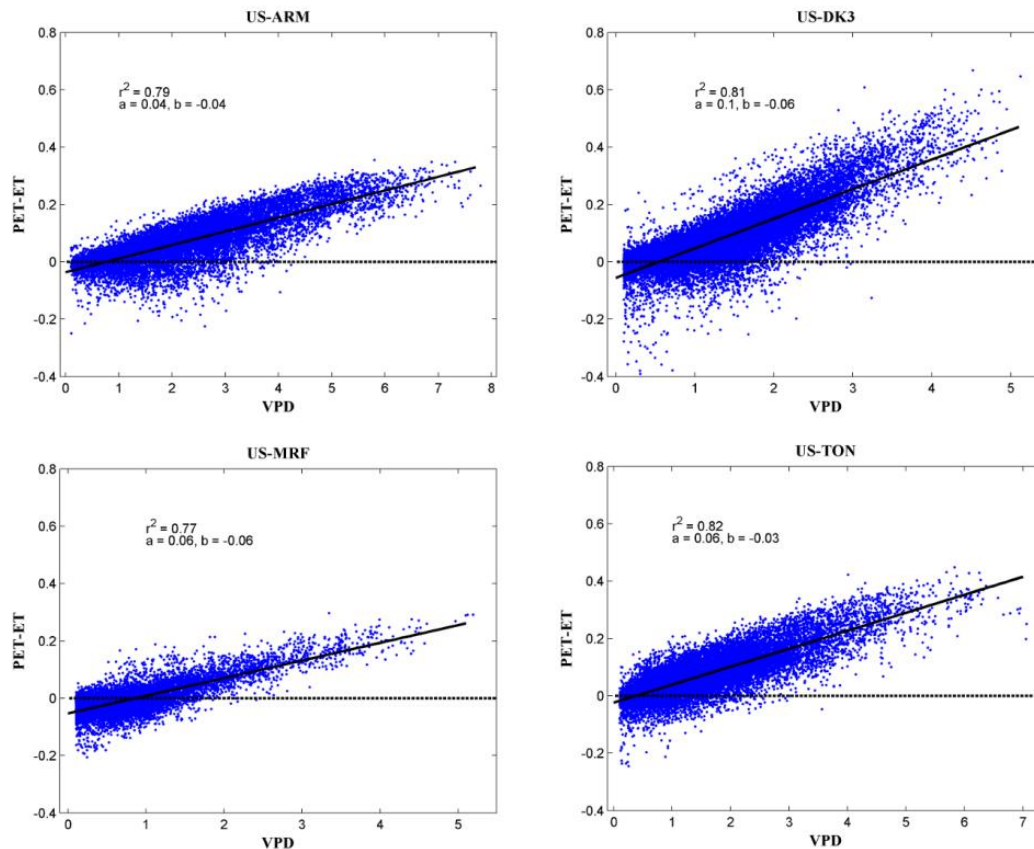
41

Figure S1: The relationship between PET-ET *(i.e. the difference between potential and observed* ET*) as a function of* VPD *for four representative sites. The slope (a) and intercept (b) of the derived linear relationship are also shown, together with the coefficient of correlation (r^2)*

Estimating the dryness index*:* The estimates of the dryness index (DI = PET/P), which rely on annual estimate of PET and P, are sensitive to missing meteorological data, and in particular missing precipitation data. As evidence, when the mean annual precipitation was determined from the hourly Level 2 Ameriflux data, the ratio of observed ET to observed precipitation (i.e. the evaporative fraction) exceeded 1.0 for about 30% of sites. A multi-year evaporative fraction greater than 1.0 is physically possible if a site experiences significant run-on soil moisture or groundwater convergence; however, in Ameriflux sites that tend to be biased to flat locations, significant run-on is not likely in most sites. Therefore, we calculated the DI using the long-term mean annual precipitation reported by each site to the Fluxnet Database (http://fluxnet.ornl.gov/) instead of calculating mean annual precipitation from the Level 2 Ameriflux data. There may be some discrepancies between the DI estimated this way and the true DI for each site's study period if the mean annual precipitation during the study period is much different than the longer-term reported average. However, because the site-specific study periods are generally long and are not limited to the same years (see Table S1), systematic biases across sites (for example due to the occurrence of a large regional drought event) should be minimal.

Section S2: Selecting the model for potential evapotranspiration (PET)

In this study, the potential evapotranspiration rate (PET) is used to calculate the dryness index, and also to quantify limitations to ET imposed by soil moisture and VPD. In many previous studies focused on understanding ecosystem hydrologic processes, the PET has been calculated using the Priestley-Taylor equation[32], which may be represented as:

$$\text{PET}_{PT} = a_{PT} \frac{S \cdot R_n}{S+\gamma} \cdot \frac{1}{\lambda_V} \qquad (S1)$$

where $a_{PT} = 1.26$ is the Priestley-Taylor coefficient, S is the temperature-dependent slope of the saturation-vapor pressure curve, γ is the temperature-dependent psychrometric constant, and λ_V is the temperature-dependent latent heat of vaporization. In this study, which is strongly focused on atmospheric limitations to ET, we estimate PET using the Penman-Monteith[33, 34] approach, which in addition to accounting for energy constraints to ET, also accounts for aerodynamic and atmospheric constraints. The Penman-Monteith equation for PET may be expressed as:

$$\text{PET}_{PM} = \frac{S \cdot R_n + c_p \rho_a g_a VPD}{\lambda_V \left[S + \gamma \left(1 + \frac{g_a}{G_S} \right) \right]} \qquad (S2)$$

where S is the temperature-dependent slope of the saturation-vapor pressure curve, R_n is net radiation, p_a is the density of dry air, γ is the temperature-dependent psychrometric constant, λ_V is the temperature-dependent latent heat of vaporization, g_a is the aerodynamic conductance, and c_p is the specific heat capacity for dry air.

The formal definition of the Penman-Monteith equation for canopy evapotranspiration relies on a big-leaf assumption, and in many applications G_S is equated to the canopy-level stomatal conductance[35]. However, ecosystem evapotranspiration includes a significant contribution from soil evaporation (typically on the order of 15-30% for a range of biomes[36, 37, 38, 39, 40]). In modeling studies, this problem is often met with a two-source (i.e. canopy and soil) modeling procedure where both canopy and soil evaporation are independently simulated from Penman-Monteith type equations. However, in data driven applications like this one, when surface conductance is derived by inverting the Penman-Monteith equation from measured ecosystem scale ET observations, the derived G_S is influenced by soil evaporation, and should not be assumed to be representative of canopy stomatal conductance alone[35, 41, 42, 43, 44]. Because soil evaporation increases linearly with VPD, a greater ratio of soil evaporation to total evapotranspiration will tend to reduce the magnitude of the VPD sensitivity parameter m.

The aerodynamic conductance (g_a) is formulated as a function of wind speed and canopy height after Campbell & Norman (1998)[45] as:

$$g_a = \frac{U \cdot k^2}{\left[\ln \left(\frac{z_m - z_d}{z_o} \right) \right]^2} \qquad (S3)$$

Where U is the measured wind speed (m/s), k is the Von Karman Constant, z_m is the measurement height, z_d is the zero plane displacement, and z_o is the momentum roughness length. The z_d and z_o where taken as $0.67h$ and $0.1h$, respectively, where h is canopy height, as is common practice in the absence of other information about these parameters[45, 46]. In some applications, it is common to incorporate a correction for stability effects on g_a via the modification:

$$g_a = \frac{U \cdot k^2}{\left[\ln \left(\frac{z_m - z_d}{z_o} \right) + \Psi_H \right]^2} \qquad (S4)$$

100

101 where the diabatic correction factor Ψ_H can be specified as a function of the ratio of convective to
102 mechanical production of turbulence as described in Campbell & Norman (1998)[45].

103 Filtering the data to remove observations collected when VPD < 0.6 kPa and wind speed < 1 m s^{-1} should
104 minimize the influence of stability effects on the derived surface conductance. To be sure, we repeated the
105 analysis in a subset of sites spanning the range of dryness index for three scenarios: 1) no stability
106 corrections to g_a (i.e. using Eq. S3) and no wind speed filter, 2) no stability corrections to g_a (i.e. using Eq.
107 S3) with the wind speed filter, and 3) stability corrections to g_a using Eq. S4 with the wind speed filter. In
108 US-DK3, the relationship between g_a and VPD was similar in all scenarios. In the other sites, the
109 relationship between g_a and VPD was similar for scenario 1 & 2, but scenario 3 resulted in higher g_a at
110 high VPD.

111 Importantly, however, regardless of which scenario was used, the relationship between G_S and VPD was
112 similar in all sites, and nearly indistinguishable in most. Thus, we elected not to correct g_a for stability
113 effects in order to minimize additional uncertainties associated with the parameterization of the stability
114 correction itself.
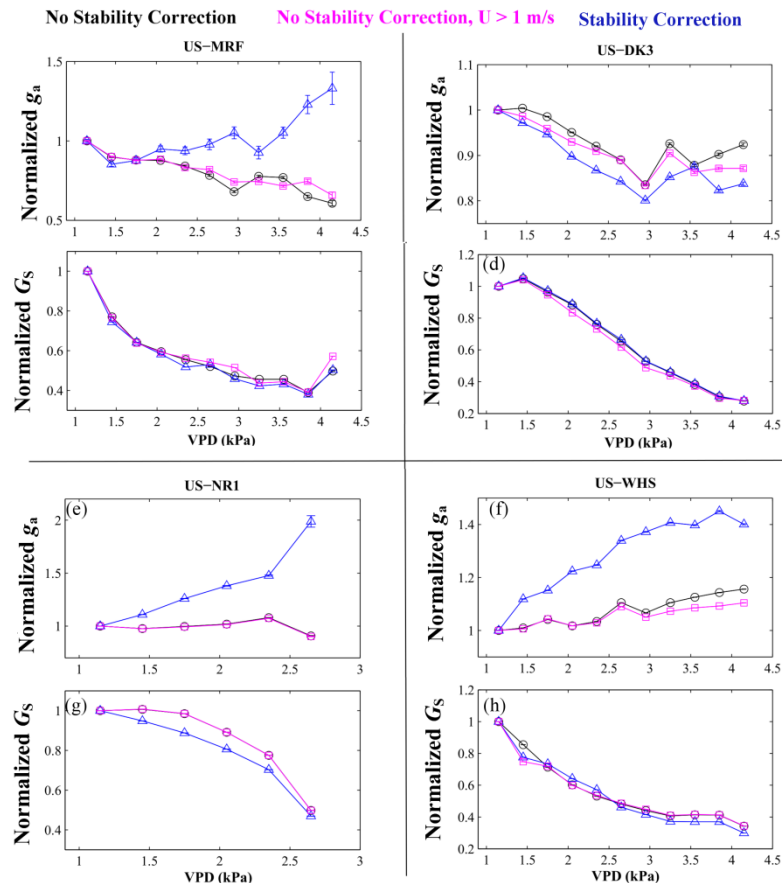

115

116   *Figure S2: The relationship between aerodynamic conductance and VPD (panels a, c, e, g), and surface*
117   *conductance (G_S) and VPD (panels b, d, f, and h), showing results from the three stability correction scenarios.*

118

119 When calculating PET_{PM} for use in determining the site dryness index, we elected to set G_S in Eq. S2
120 equal to .0148 m/s. This represents the highest value of the reference, well-watered surface conductance
121 rate (i.e. $G_{S,ref,ww}$) observed across the study domain. This approach of using a finite G_S to determine PET
122 is conceptually consistent with the use of the Priestly-Taylor equation, since the parameter a_{PT} is set to
123 approximate well-watered evapotranspiration rates from terrestrial ecosystems, and not, for example,
124 open water (over which G_S is infinite).

125 The agreement between the dryness index calculated using PET_{PT} and PET_{PM} is shown for reference in
126 Figure S3. The dryness index values tend to be higher when calculated using the Penman-Monteith
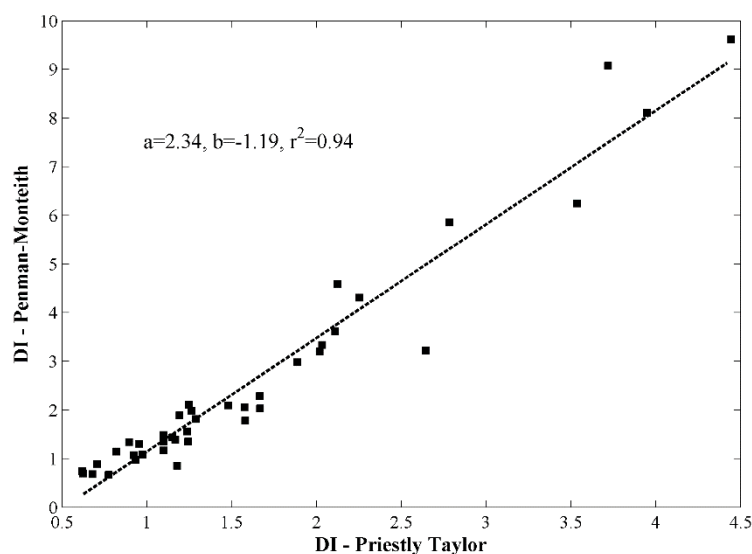127 equation, but overall the two estimates of PET are strongly correlated.

128

129 *Figure S3: The relationship between dryness index estimated using the Penman-Monteith and Priestly-Taylor*
130 *Models for PET.*

131

132

133

134

135

136

137

138

139

140

141

142

Section S3: The use of soil moisture content as an indicator of plant water availability

145 We elected to use the total volumetric soil moisture (θ) in the top 30 cm as the primary proxy for plant
146 water availability. Most Ameriflux sites rely on time-domain reflectometry (TDR) measurements for θ,
147 which often require a site-specific calibration. Details of these site-specific calibrations are not available
148 in the Ameriflux database, and thus cross-site comparisons of soil moisture content should be approached
149 with caution. In other studies, the relative extractable water (REW, which represents soil moisture content
150 scaled by the minimum and maximum observed values) is used instead to facilitate cross-site comparisons
151 of ecosystem water use[47, 48].

152 It could be argued that soil water potential (Ψ_S) is a more appropriate measure of soil water availability
153 than either θ or REW, since water tension in the soil is an important physical driver of water movement
154 through soil matrices and plants[49, 50]. Unfortunately, soil water potential is rarely measured in the field.
155 Occasionally, laboratory-based dry down experiments are used to derive an empirical relationship
156 between θ and Ψ_S. This relationship is not linear[49], though it is monotonically increasing. As illustrated in
157 Figure S4, in sites for which estimates of Ψ_S are available, Ψ_S increases more rapidly with increasing θ
158 when the latter is low; consequently, the results of this study associated with the drier soil moisture bins
159 will likely reflect the response to a relatively wider range of Ψ_S conditions.

160 It is important to note that the choice of the soil moisture variable (i.e. θ vs. REW vs. Ψ_S) has no effect on
161 our primary results concerning the relative importance of soil moisture versus VPD limitations to surface
162 conductance and ET (e.g. the results presented in Figures 2, 3 & 4 in the main text). This is because the
163 analytical approach relies on binning the data into quantiles defined by the 0-15th, 15th-30th, 30th-50th, 50th-
164 70th, 70th-90th, and 90th-100th percentiles of θ, and then parameterizing Eq. 1 within each bin. Because the
165 relationships between θ and REW and Ψ_S are all monotonically increasing, the same data will fall into the
166 same bins regardless of which soil moisture metric is used.
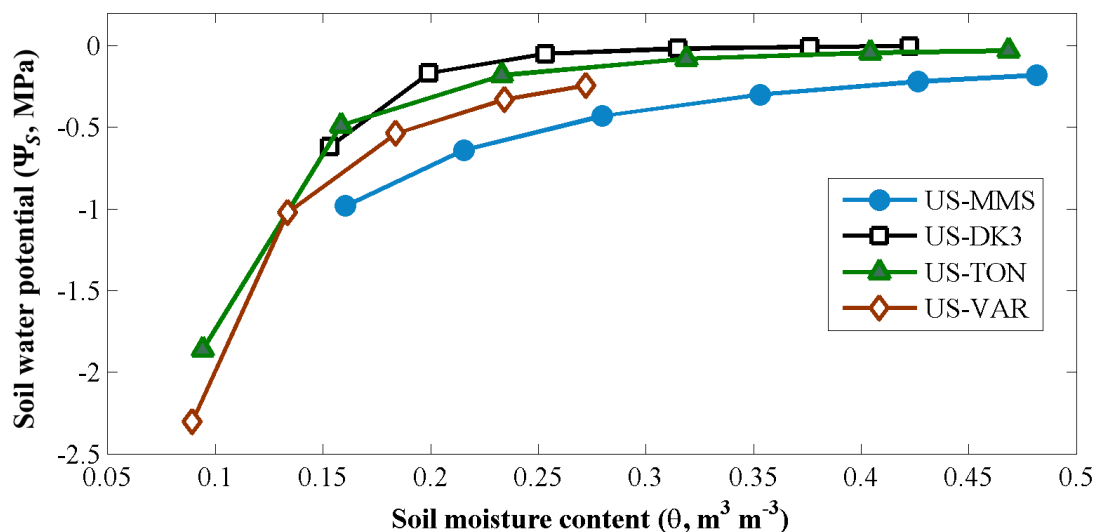
167

168 *Figure S4: The relationship between soil water potential (Ψ_S) and soil moisture content (θ) in four study sites for*
169 *which site-specific relationships between θ and Ψ_S were available (see references Wayson et al. 2016 for US-MMS,*
170 *Hacke et al. 2000 for US-DK3, and Baldocchi et al. 2004 for US-TON and US-VAR.*

171

172

173 ## S4. Determining the well-watered reference surface conductance (i.e. $G_{S,ref,ww}$).

174 The limitations to G_S imposed by soil moisture and VPD were estimated by comparing hourly estimates
175 of G_S to the well-watered reference value of surface conductance (i.e. $G_{S,ref,ww}$). This parameter represents
176 the surface conductance when soil moisture content exceeds the 90th percentile in each site, and 0.9 <
177 VPD < 1.1 kPa. Choosing the reference VPD of 1.0 kPa is consistent with previous work[31]. The approach
178 recognizes the fact that surface conductance estimates at low VPD are sensitive to biases introduced by
179 low boundary layer conductance and instabilities in the determination of G_S from ET when VPD is low.

180 The magnitude of $G_{S,ref,ww}$ tends to be low in sites with a high dryness index, and variable but generally
181 higher in more mesic sites (Figure S5). The low $G_{S,ref,ww}$ in the driest sites is expected, as canopy stomatal
182 conductance – an important component of G_S - is driven by leaf area[51], which is very low in semi-arid
183 ecosystems. The variability in $G_{S,ref,ww}$ in more mesic sites may be explained, to an extent, by variation in
184 leaf area as well as variation in canopy height, which introduces another important structural control on
185 canopy stomatal conductance[30, 52]. While these sources of variability in well-watered G_S are an important
186 long-term constraint on ecosystem carbon and water cycling, they are not the focus of this present study.
187 We point readers elsewhere[32] for a more thorough treatment of the topic.
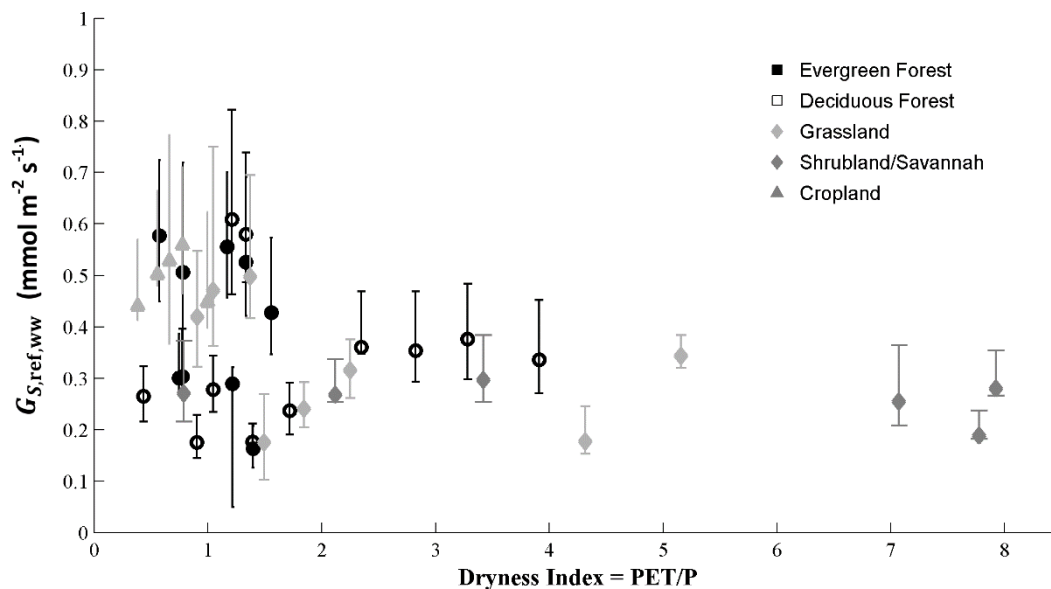

188

189 *Figure S5: The relationship between the well-watered reference surface conductance ($G_{S,ref,ww}$) and dryness index.*
190 *Error bars indicates the 50% confidence interval on the estimate of $G_{S,ref,ww}$ as derived from a non-parametric*
191 *bootstrap.*

192

193

194

195

196

197

198

Section S5: The relationship between VPD and θ at various timescales

200 Our analysis leverages the fact that while VPD and θ are moderately to strongly correlated at long time-
201 scales (i.e. monthly to annual), they are relatively weakly coupled at the hourly and daily timescales over
202 which Ameriflux data is gathered. In Figure 1 of the main text, we present a summary of the correlation
203 between θ and VPD averaged across all study sites for varying averaging periods (i.e. seasonal, monthly,
204 weekly, daily, and hourly). For illustrative purpose, we show the data that inform that summary
205 presentation for one representative site in Figure S6, and present the statistics of the linear regressions
206 between the two variables over the various timescales in Table S2.
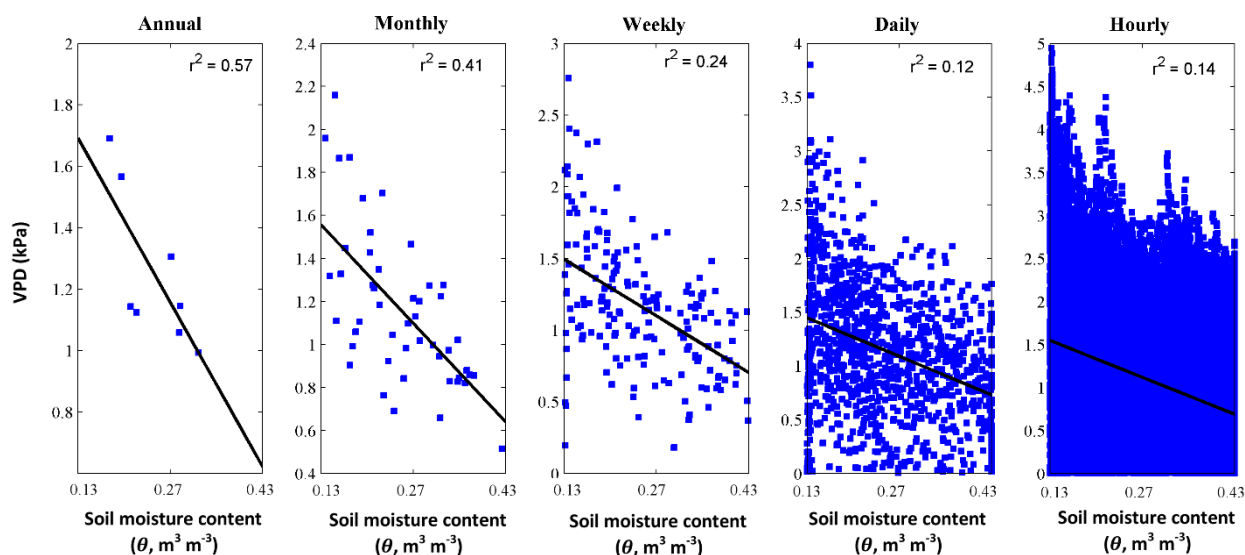

207
208 *Figure S6: The relationship between vapor pressure deficit (*VPD*) and soil moisture content (*θ*) when both are*
209 *averaged over various timescales. Data are from the US-DK3 (Duke Pine Forest).*

210
211
212
213
214
215
216
217
218
219
220
221
222
223
224
225
226

227

228

229 *Table S2: The slope, intercept, and correlation coefficient of the relationship between vapor pressure deficit (VPD)*
230 *as a linear function of soil moisture content (θ) inferred by averaging the data over various timescales. In general,*
231 *the slope and intercept parameters are relatively stationary across timescales, but the two variables become*
232 *increasingly decoupled (i.e. r^2 is lower) at shorter timescales.*

	Slope					Intercept					correlation coefficient (r^2)				
	year	month	week	day	hour	year	month	week	day	hour	year	month	week	day	hour
ARM	-0.91	-1.10	-1.28	-1.36	-0.98	2.54	2.54	2.70	2.76	1.96	0.38	0.12	0.15	0.14	0.06
BAR	-0.46	-0.13	-0.24	-0.24	-0.37	1.15	0.97	1.00	0.98	0.94	0.55	0.02	0.04	0.02	0.03
BLK	-0.65	-0.32	-0.47	-0.60	-0.19	1.73	1.50	1.63	1.67	1.06	0.40	0.04	0.07	0.04	0.01
BLO	0.18	-0.81	-0.39	-0.21	-1.16	1.80	1.95	1.90	1.89	2.08	0.08	0.20	0.04	0.01	0.32
BO1	-0.41	-0.44	-0.63	-0.48	-0.29	1.30	1.36	1.45	1.28	1.01	0.26	0.22	0.24	0.10	0.01
BR3	0.73	0.27	-0.31	-0.50	0.13	0.62	0.94	1.22	1.28	0.88	0.65	0.10	0.09	0.15	0.00
DK1	-1.40	-0.96	-1.04	-0.96	-0.82	1.83	1.60	1.66	1.60	1.53	0.67	0.40	0.31	0.19	0.13
DK2	-1.79	-0.94	-1.08	-1.01	-0.78	1.97	1.57	1.65	1.61	1.53	0.81	0.36	0.31	0.21	0.13
DK3	-1.07	-0.92	-0.79	-0.72	-0.86	1.69	1.56	1.49	1.45	1.55	0.57	0.42	0.25	0.12	0.15
FMF	0.10	-0.56	-0.65	-1.09	-0.88	1.55	1.82	1.94	2.25	1.79	0.01	0.07	0.09	0.12	0.08
FR2	-1.70	-0.92	-1.50	-1.30	-1.13	2.42	1.98	2.34	2.21	2.00	0.98	0.18	0.55	0.33	0.14
FUF	-1.25	-1.20	-1.32	-1.43	-0.91	2.18	2.09	2.20	2.25	1.66	0.95	0.64	0.57	0.40	0.16
GLE	0.06	0.03	0.13	0.14	0.61	0.96	0.93	0.91	0.90	0.20	0.03	0.01	0.04	0.01	0.16
IB1	-0.64	-0.56	-0.65	-0.79	-1.10	1.52	1.45	1.51	1.57	1.62	0.56	0.30	0.42	0.29	0.16
IB2	-0.45	-0.53	-0.44	-0.61	-0.84	1.40	1.39	1.36	1.46	1.39	0.24	0.23	0.12	0.10	0.10
KFS	-2.75	-1.60	-1.66	-1.52	-1.67	2.74	2.02	2.16	2.16	2.17	0.99	0.34	0.36	0.25	0.28
KON	-0.68	-1.42	-1.41	-1.21	-1.23	2.05	2.41	2.49	2.34	2.10	0.49	0.32	0.28	0.18	0.14
KSO	0.25	0.10	-0.09	-0.20	-0.22	1.10	1.11	1.20	1.22	1.25	0.03	0.00	0.00	0.01	0.01
ME2	-0.48	-0.68	-0.38	-0.61	-1.27	1.63	1.53	1.51	1.64	1.78	0.11	0.07	0.02	0.04	0.32
ME3	0.62	-0.48	-0.37	-0.63	-1.38	1.79	2.00	2.03	2.17	2.11	0.06	0.08	0.02	0.04	0.28
MMS	-0.96	-0.42	-0.29	-0.33	-0.78	1.52	1.18	1.09	1.12	1.32	0.43	0.13	0.05	0.04	0.11
MOZ	-0.67	-0.82	-0.93	-1.02	-1.09	1.71	1.75	1.84	1.89	1.69	0.28	0.26	0.27	0.19	0.15
MRF	0.66	-0.76	-0.66	-0.59	-0.72	0.50	0.94	0.93	0.89	0.99	0.09	0.52	0.27	0.10	0.17
NC2	-0.24	-0.27	-0.21	-0.27	-0.45	1.34	1.30	1.28	1.30	1.29	0.48	0.12	0.04	0.03	0.04
NE1	-0.96	-0.98	-0.80	-1.03	-0.20	1.77	1.77	1.66	1.80	1.15	0.30	0.33	0.21	0.18	0.00
NE3	-1.52	-0.84	-0.58	-0.73	-0.57	1.97	1.69	1.58	1.65	1.42	0.56	0.32	0.18	0.15	0.04
NR1	-0.31	-0.25	-0.38	-0.38	-0.05	1.07	1.03	1.07	1.08	0.66	0.27	0.17	0.16	0.06	0.00
OHO	-1.58	-0.86	-0.63	-0.57	-0.86	1.79	1.42	1.34	1.31	1.33	0.47	0.35	0.19	0.11	0.15
SRC	0.82	-1.09	-1.08	-1.11	-1.18	2.25	2.98	3.03	3.02	2.92	0.27	0.10	0.10	0.09	0.07
SRG	-1.17	-1.90	-1.73	-1.73	-1.95	2.90	3.13	3.07	3.09	3.14	0.64	0.45	0.34	0.24	0.33
SRM	-1.61	-0.80	-1.22	-1.38	-1.72	3.04	2.74	2.93	2.99	2.85	0.17	0.07	0.20	0.20	0.22
SYV	0.04	-0.16	-0.13	-0.08	-0.51	1.00	1.03	1.06	1.04	1.11	0.00	0.02	0.01	0.00	0.04
TON	-0.33	-0.27	-0.45	-0.51	-0.64	0.88	0.83	0.90	0.91	1.06	0.47	0.05	0.12	0.11	0.08
UMB	0.09	-0.95	-0.69	-0.68	-0.80	0.88	1.25	1.15	1.13	1.20	0.03	0.54	0.30	0.18	0.17
VAR	-0.32	-0.57	-0.51	-0.56	-0.56	0.87	0.98	0.93	0.95	0.98	0.17	0.27	0.18	0.13	0.09
WBW	-0.83	-0.22	-0.30	-0.41	-0.59	1.52	1.12	1.18	1.23	1.32	0.13	0.03	0.05	0.06	0.07
WCR	0.12	0.04	-0.06	-0.16	0.02	0.47	0.49	0.56	0.60	0.41	0.05	0.00	0.00	0.01	0.00
WHS	-2.49	-0.69	-1.38	-1.49	-0.95	3.65	2.76	3.17	3.24	2.61	0.51	0.03	0.16	0.17	0.05
WKG	-0.03	-1.05	-1.09	-1.16	-0.99	2.38	2.63	2.77	2.82	2.41	0.00	0.12	0.15	0.13	0.06
Mean	-0.62	-0.67	-0.71	-0.76	-0.77	1.68	1.63	1.69	1.71	1.55	0.36	0.20	0.18	0.13	0.12
Std	0.84	0.47	0.48	0.46	0.52	0.71	0.65	0.69	0.70	0.66	0.29	0.17	0.14	0.09	0.09

233
234

235

236

237

238

239

240

Section S6: Determining soil moisture as compared to VPD constraints to G_S and ET: The growing season ET and meteorological data were sorted into bins representing the 0-15th, 15th-30th, 30th-50th, 50th-70th, 70th-90th, and 90th-100th percentiles of θ, spanning a gradient of dry to wet conditions in each site. Within each soil moisture bin, we further sorted the data on the basis of VPD; the VPD bins had a width of 0.2 kPa, and there were $j = 1,2….N_i$ VPD bins in each soil moisture bin, where N_i varies as a function of the maximum VPD observed at each site. The mean G_S in each bin was determined provided there were more than 10 data points in any given (i,j) bin.

The binned averages were used to derive site- and soil-moisture-specific parameterizations for Eq. 1 in the main text, which were leveraged to quantify the total growing season average supply and demand limitations to G_S and ET. Briefly, θ constraints were inferred from changes in the intercept parameter ($G_{S,ref}$), and VPD constraints were inferred from the sensitivity parameter m. Estimates of hourly G_S reflecting either θ or VPD control for all daytime periods were then subtracted from the $G_{S,ref,ww}$ to quantify the magnitude of limitations to G_S attributable to each driver. These estimates of hourly G_S were then used in Eq. S2 to generate estimates of ET that reflect either θ of VPD constraints to G_S. Limitations to ET were then defined as the difference between hourly PET and ET, where the PET is generated using Eq. S2 forced with the site-specific $G_{S,ref,ww}$. In most sites, the reported θ corresponds to integrated observations over the top 30 cm of the soil. The soil moisture dynamics in the top 30 cm may not always be well coupled to soil moisture at depth, which represents a potential source of bias in sites with deeper roots.

In Figure 2 of the main text, we show representative results from four sites. Here are analogous figures for all study sites. The fitted lines, which show the model of Eq. 1 within each soil moisture bin, do not extend below VPD < 1.0 kPa, as those data were not used to drive the regressions due again to instabilities in the observations at low VPD.
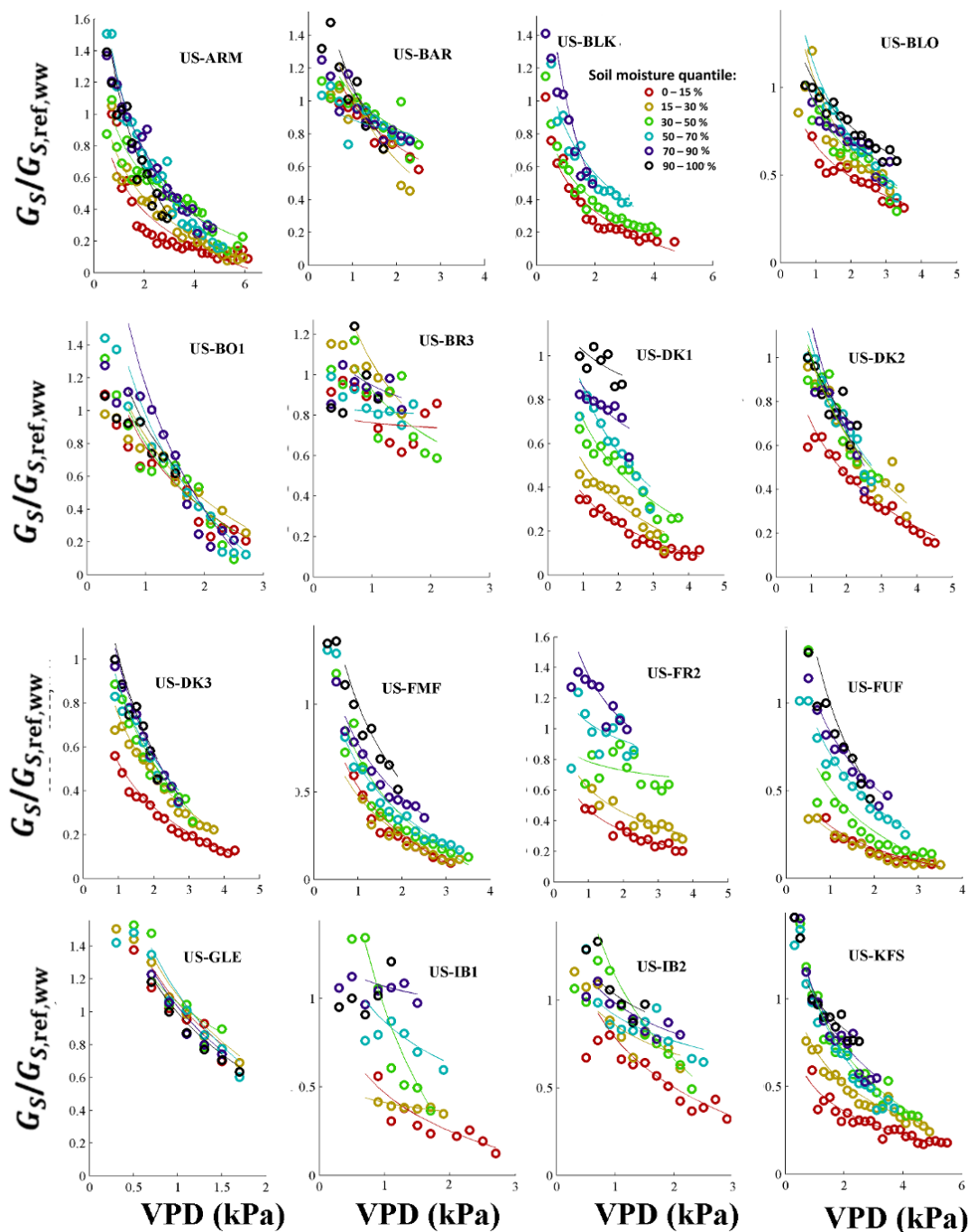
266

267
268   *Figure S7. Same as Figure 2a-d in the main text, but for the first sixteen study sites (in alphabetical order).*
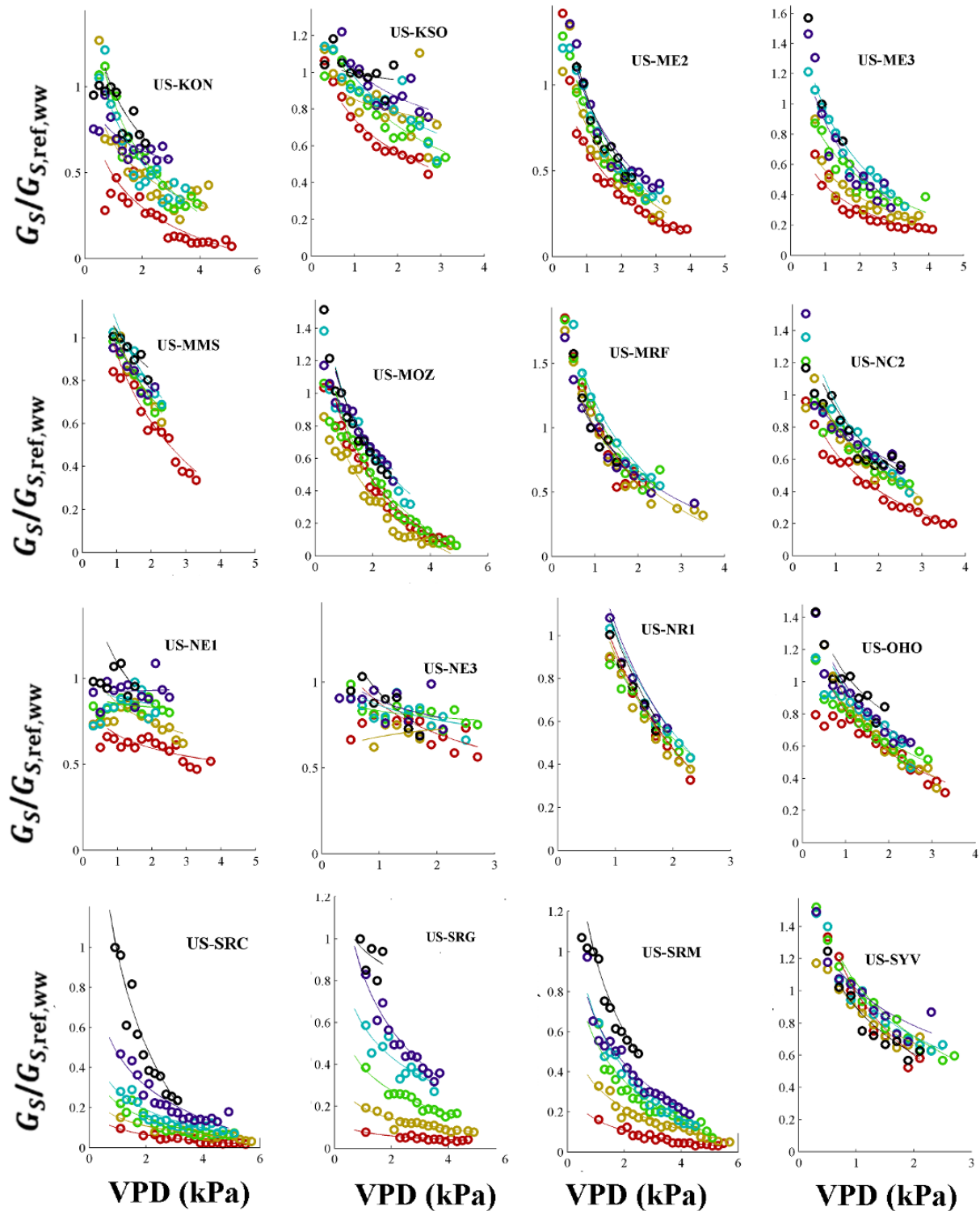
269
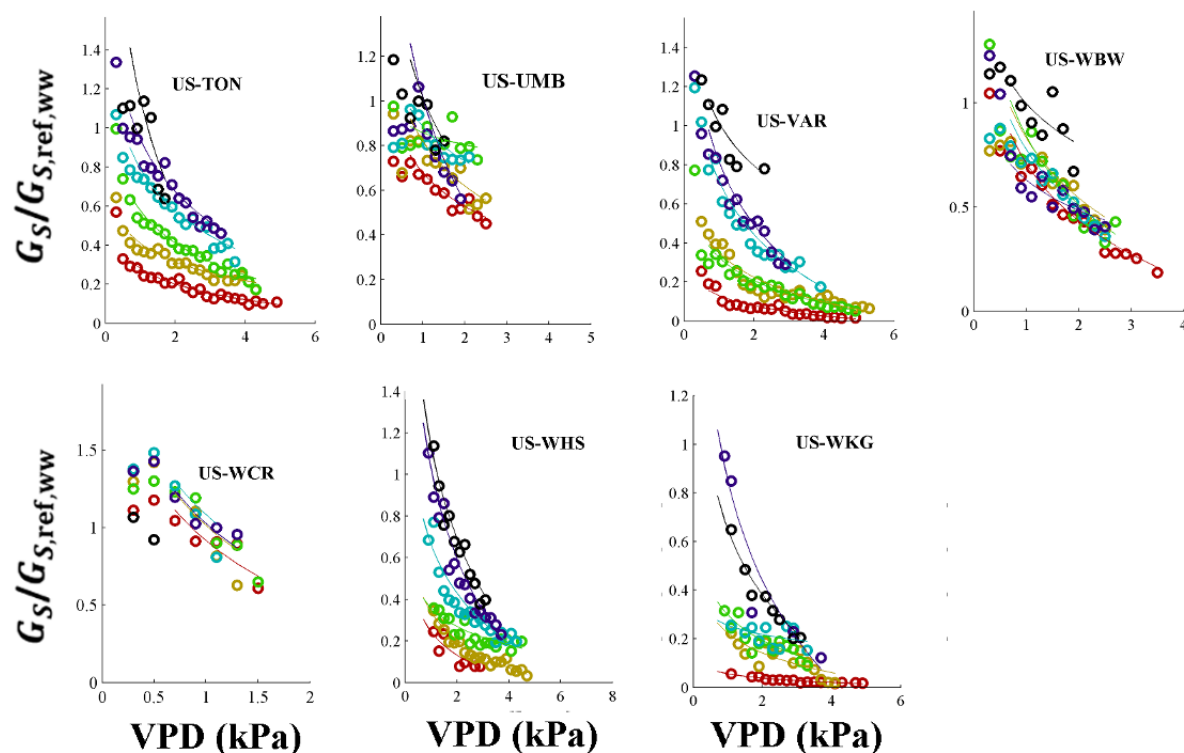270 *Figure S8. Same as Figure 2a-d in the main text, but for the second sixteen study sites (in alphabetical order).*
271
272
273
274

275
276   *Figure S9. Same as Figure 2a-d in the main text, but for the last seven study sites (in alphabetical order).*

277

278

279

280

281

282

283

284

285

286

287

288

289

290

291

Section S7: Effects of other meteorological drivers on $G_{S,ref}$

292

293 Other work has demonstrated that the reference surface or stomatal conductance may be sensitive to
294 variations in photosynthetically active radiation (PAR) and air temperature (T_a)[51, 53]. In this study,
295 variations in $G_{S,ref}$ with PAR or T_a were not explicitly considered, due primarily to the fact that accounting
296 for them (for example, by introducing additional dimensions to the data binning matrix) often results in an
297 insufficient amount of data within each soil moisture bin to properly parameterize Eq. 1. This is
298 particularly true in sites with a short active season, which include both the hottest and coolest sites in the
299 dataset.

300 In all sites, VPD is directly correlated with temperature (reflecting the fact that the saturation vapor
301 pressure depends exponentially on T_a), and also directly correlated with PAR (since T_a tends to be highest
302 when radiation loads are high, see Figure S10). Soil moisture tends to be inversely correlated with T_a in
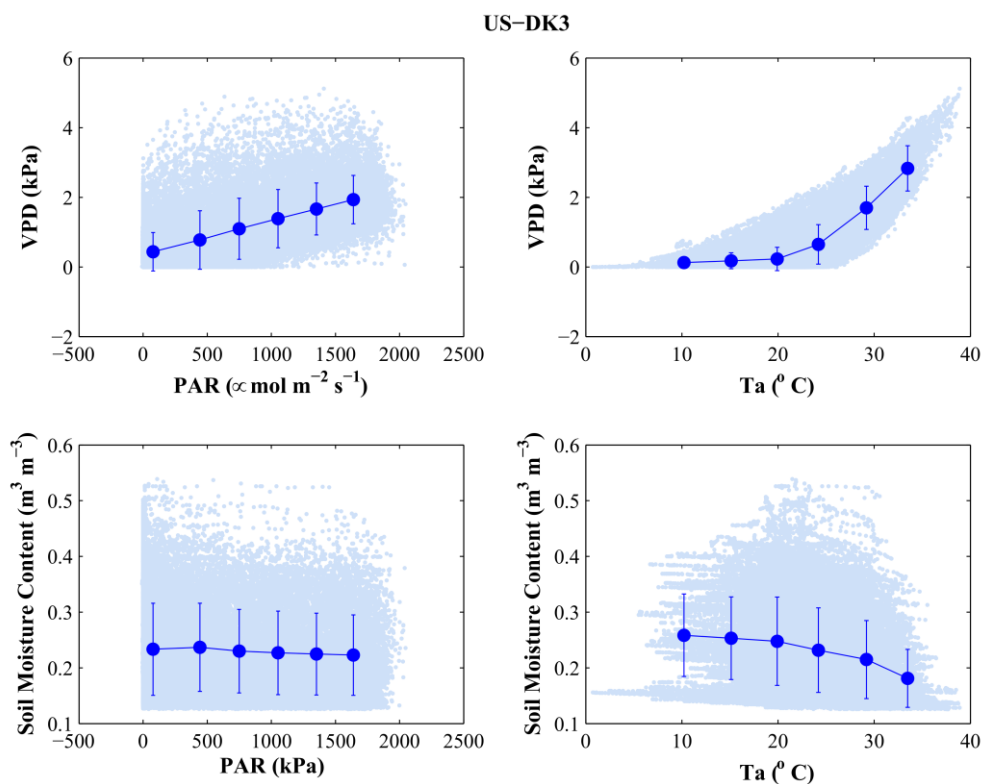303 most sites, and only weakly related to PAR (again, see Figure S10).

304

305 *Figure S10: The relationship between vapor pressured deficit (VPD), photosynthetically active radiation (VPD) and*
306 *air temperature (T_a) at the Duke Forest pine plantation (US-DK3). Light blue dots show all data, and blue circles*
307 *show binned averages. Error bars show one standard deviation.*

308

309 It is possible that high T_a may limit G_s and ET through biochemical imitations to leaf-level gas exchange[54]
310 that occur independent of limitations to G_s imposed by high VPD. In that case, failure to resolve
311 temperature effects on G_s could lead us to overestimate the VPD limitations and underestimate the soil
312 moisture limitations. On the other hand, because canopy stomatal conductance is known to be

313 monotonically related to PAR[51, 55], failure to account for independent PAR effects could lead us to
314 underestimate VPD limitations and overestimate soil moisture limitations.

315 To explore the extent to which these biases are significant, in each site, we attempted separate
316 parameterizations for Eq. 1 when PAR was limited to high values (PAR > 1500 µmol m^{-2} s^{-1}) and when T_a
317 was limited to a relatively narrow range of 5 ^{o}C. In both cases, data were binned according to soil
318 moisture content as described in the methods of the main text. The range of temperature depended on the
319 mean growing season T_a at each site but was usually between 20 and 25 ^{o}C. Enough growing season data
320 were available to support this effort in 23 of the sites. In general, the $G_{s,ref,j}$ (i.e. $G_{S,ref}$ for each of the j=6
321 soil moisture bins) were similar regardless of whether the full or filtered datasets were used (see Fig S11
322 for results from representative sites). Specifically, across all sites, the slope of the relationship between
323 the $G_{s,ref}$ values obtained from the full dataset as compared to the dataset filtered to a narrow temperature
324 range was 0.97 on average (st. dev. = 0.44), and the average correlation coefficient was 0.75. Similarly,
325 the slope of the relationship between the $G_{S,ref}$ values obtained from the full dataset as compared to the
326 dataset filtered to a PAR range was 1.02 on average (std dev. = 0.40), and the average correlation
327 coefficient was 0.80. Thus, the decision not to account for PAR and T_a effects on $G_{S,ref}$ does not introduce
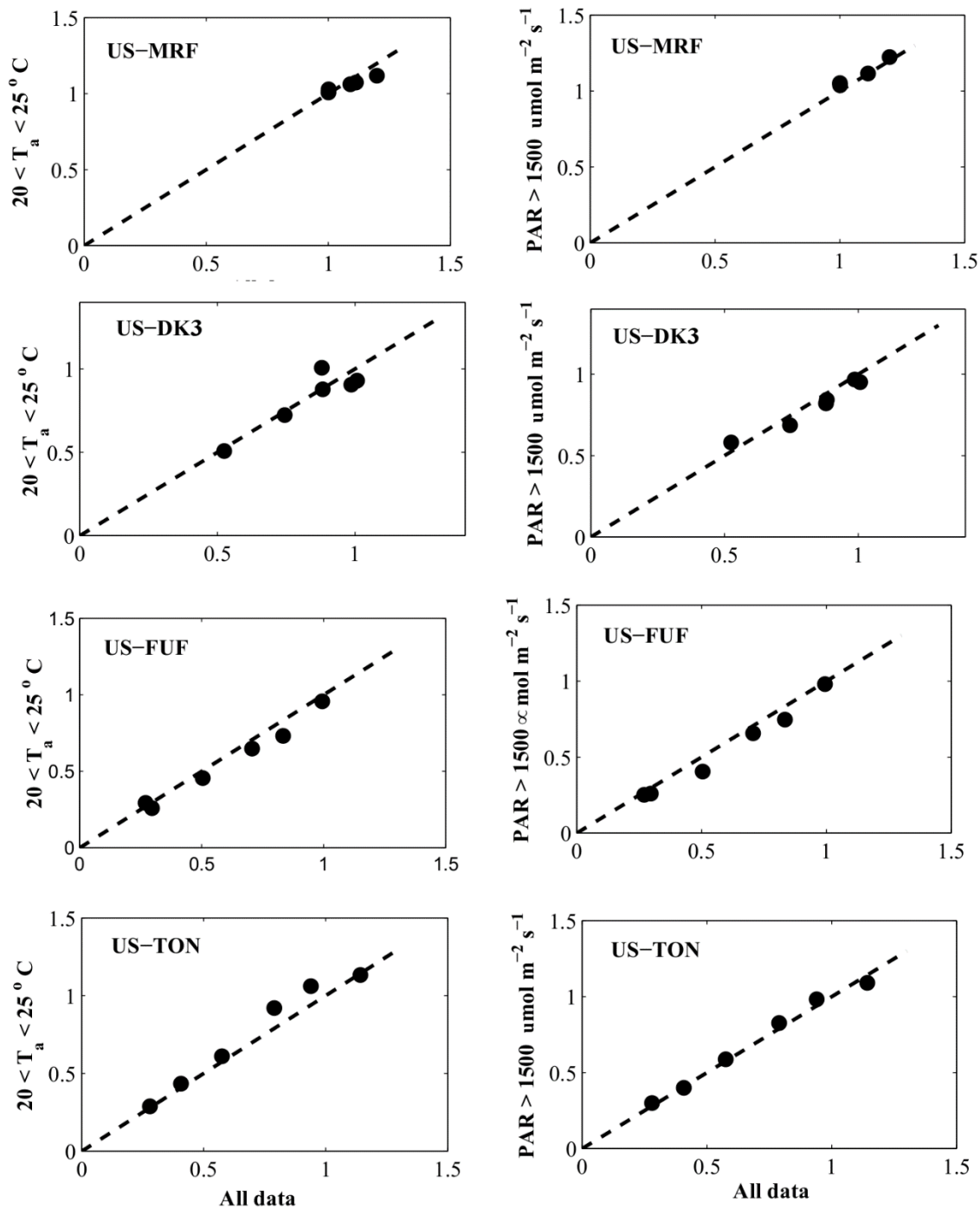328 systematic biases across the sites.

329

330 *Figure S11: The relationship between the reference G_s within each soil moisture bin (i.e. $G_{s,ref,j}$) as derived from all*
331 *growing season data (subject to the filtering constraints described in Section S1), and data subjected to an*
332 *additional temperature filter (left hand column) or PAR filter (right hand column). The sites shown here span a*
333 *range of dryness index (see Table S1).*

334

Section S8: Future projections – model estimates and downscaling

336 Projections for future meteorological variables, including R_n, VPD, air temperature, and precipitation
337 were obtained from ten general circulation models for the period from 2071-2080, chosen as the transition
338 point between the mid- and late-21st century. Modeled data were downscaled in space using parametric
339 approaches, and downscaled in time using representative diurnal patterns measured at each study site.
340 Future soil moisture was estimated from a marginal distribution sampling approach based on short- and
341 long-term dynamics of VPD and precipitation that reproduced observed soil moisture dynamics with little
342 bias. The future VPD and soil moisture limitations to G_S and ET were then determined in a matter
343 analogous to the approach for present day conditions.

344 ***Obtaining projections of future meteorological drivers***: Estimates of the key drivers of the Penman-
345 Monteith model were obtained from the Multivariate Adaptive Constructed Analogs (MACA[56]) data
346 warehouse (http://maca.northwestknowledge.net/) for a representative selection of twelve Ameriflux sites
347 that include long-running towers and that span a wide gradient in climate (See Table S1). Specifically, we
348 obtained daily time series of net radiation, air temperature, specific humidity, and wind speed projected
349 from 10 General Circulation Models from the Coupled Model Intercomparison Project – Phase 5
350 (CMIP5) archive driven by representative concentration pathway 8.5 (highest greenhouse gas emission
351 scenario) were downloaded for the period 1950-2099. The ten models are listed in Table S3.

352 Table S3: The models used to obtain estimates of future meteorological drivers

Model Name	Model Country	Model Agency
CanESM2	Canada	Canadian Centre for Climate Modeling and Analysis
CNRM-CM5	France	National Centre of Meteorological Research, France
CSIRO-Mk3-6-0	Australia	Commonwealth Scientific and Industrial Research Organization/Queensland Climate Change Centre of Excellence, Australia
GFDL-ESM2G	USA	NOAA Geophysical Fluid Dynamics Laboratory, USA
HadGEM2-ES	United Kingdom	Met Office Hadley Center, UK
inmcm4	Russia	Institute for Numerical Mathematics, Russia
IPSL-CM5A-LR	France	Institut Pierre Simon Laplace, France
MIROC-ESM-CHEM	Japan	Japan Agency for Marine-Earth Science and Technology, Atmosphere and Ocean Research Institute (The University of Tokyo), and National Institute for Environmental Studies
MIROC5	Japan	Atmosphere and Ocean Research Institute (The University of Tokyo), National Institute for Environmental Studies,and Japan Agency for Marine-Earth Science and Technology

353

354 ***Spatial downscaling of the model data***: While the MACA CMIP data have already been downscaled
355 with respect to the climate models, the spatial resolution of these data (4 km x 4 km) still exceeds the size
356 of a typical flux footprint (typically <1 square km during the daytime). Furthermore, significant biases
357 were observed between the CMIP and observed meteorological drivers. Thus, the meteorological data
358 were further downscaled using a parametric approach driven by the site-level observations.

359   Specifically, for air temperature, VPD, R_n, and wind speed, histograms of the downscaled GCM data for
360   the period coincident with the study period at each site were compared to histograms of the measured data
361   after the latter was aggregated to daily averages to match the temporal resolution of the modeled data.
362   Biases were removed by first log-transforming both datasets, and then determining the mean and standard
363   deviation of the resulting log-normal distributions. The modeled time series were then further transformed
364   to a standard log-normal variable that was then scaled using the mean and standard deviation of the log-
365   transformed measured time series, and exponentiated (hereafter the "modeled$_{present,scaled}$" data). This
366   downscaling was performed separately for each model.

367   Next, the modeled meteorological time series for the period 2071-2080 were extracted as representative
368   of the mid-to-late 21st century. The shift in the mean of each modeled variable between the measurement
369   ("present") time period and the future was determined from the unscaled daily projections according to:

370   $$\mu_{\text{factor}} = \left(\frac{\text{mean}[\ln(\text{modeled}_{2071-2080})]}{\text{mean}[\ln(\text{modeled}_{present})]} \right) \tag{S4}$$

371   $$\sigma_{\text{factor}} = \left(\frac{\text{stdev}[\ln(\text{modeled}_{2071-2080})]}{\text{stdev}[\ln(\text{modeled}_{present})]} \right) \tag{S5}$$

372   The time series for the period 2071-2080 was then transformed into a standard normal variable that was
373   scaled using the mean and standard deviation of the modeled$_{present,scaled}$ distributions after correcting those
374   moments by μ-factor and σ-factor, respectively. This approach preserves the projected relative changes in
375   the mean and variance of the modeled time series between the present and future conditions, but retains
376   the spatial downscaling to the site level.

377   ***Projecting future relative extractable soil water:*** Projections of downscaled soil moisture were not
378   available from the MACA data warehouse. Thus, future soil moisture (at a daily time step) was estimated
379   using a site-specific marginal distribution sampling approach (i.e. a look-up table), similar to the
380   approaches frequently used to gapfill missing eddy covariance data[57]. Accordingly, measured θ data were
381   binned according to the following classification scheme, which depends on the total time since a
382   significant rain event (>20 mm), among other hydrologic variables:

383   *1) If the time since a significant (>20 mm) rain event is less than two days, then soil moisture is the*
384   *mean of measured values when:*
385   ▪ *The total precipitation within the last 7 days agrees to within 10 mm*
386   ▪ *The day-of-year agrees to within 10 days;*

387   *else, 2) If the time since a significant (>20 mm) rain event is between 2 and 3 days, then soil moisture is*
388   *the mean of measured values when:*
389   ▪ *The total precipitation within the last 30 days agrees to 20 mm*
390   ▪ *The total precipitation within the last 7 days agrees to 10 mm*
391   ▪ *The mean* VPD *within the last 30 days agrees to within 0.15 kPa*
392   ▪ *The day-of-year agrees to within 10 days;*

393   *else, 3) If the time since a significant (>20 mm) rain event is greater than three days, then soil moisture is*
394   *the mean of measured values when:*
395   ▪ *The time since a significant rain event agrees to within 5 days*
396   ▪ *The total precipitation within the last 30 days agrees to 20 mm*
397   ▪ *The total precipitation within the last 7 days agrees to 10 mm*
398   ▪ *The mean* VPD *within the last 30 days agrees to within 0.15 kPa*
399   ▪ *The day-of-year agrees to within 10 days*

400　Most of the data fall into category three. We found that it was sometimes necessary to iteratively relax the
401　search criteria in order to obtain at least two observations of soil moisture that match the criteria for every
402　hourly or half-hour observation in the record. Specifically, for category three data, the criteria were
403　loosened as follows:

404　ITERATION 2:
405　　▪　*The time since a significant rain event agrees to within 8 days*
406　　▪　*The total precipitation within the last 30 days agrees to 30 mm*
407　　▪　*The total precipitation within the last 7 days agrees to 20 mm*
408　　▪　*The mean* VPD *within the last 30 days agrees to within .25 kPa*
409　　▪　*The Julian day of year agrees to within 20 days*

410　ITERATION 3:
411　　▪　*The time since a significant rain event agrees to within 10 days*
412　　▪　*The total precipitation within the last 30 days agrees to 40 mm*
413　　▪　*The total precipitation within the last 7 days agrees to 30 mm*
414　　▪　*The mean* VPD *within the last 30 days agrees to within 0.4 kPa*
415　　▪　*The day-of-year agrees to within 180 days*

416　ITERATION 4:
417　　▪　*The mean* VPD *within the last 30 days agrees to within 0.4 kPa*

418　Any remaining gaps in the modeled θ record were linearly interpreted.

419　In general, the marginal distribution sampling approach reproduced measured θ time series very well. A
420　representative case is shown in Figure S10 and S11 for US-DK3, the Duke Pine Forest Site. Figure S12
421　shows the slope and correlation coefficient (r^2) between the measured and modeled θ for all sites used in
422　this portion of the analysis. Biases in the slope were less than 5% in most sites, and correlation was
423　generally between 0.8 and 1.0.

424

425

426

427

428

429
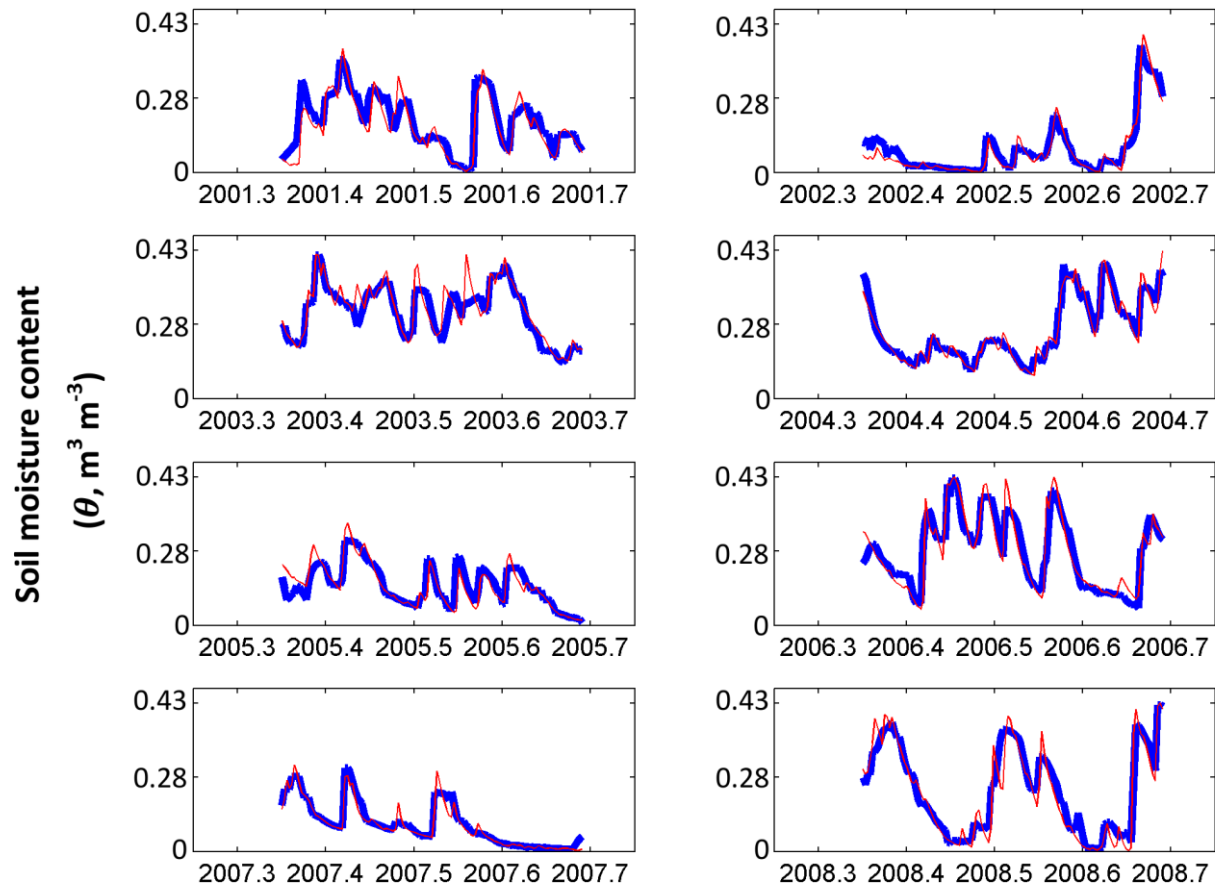
430
431

432 *Figure S10: The measured (red) and modeled (blue line) trends in growing season, daily-averaged soil*
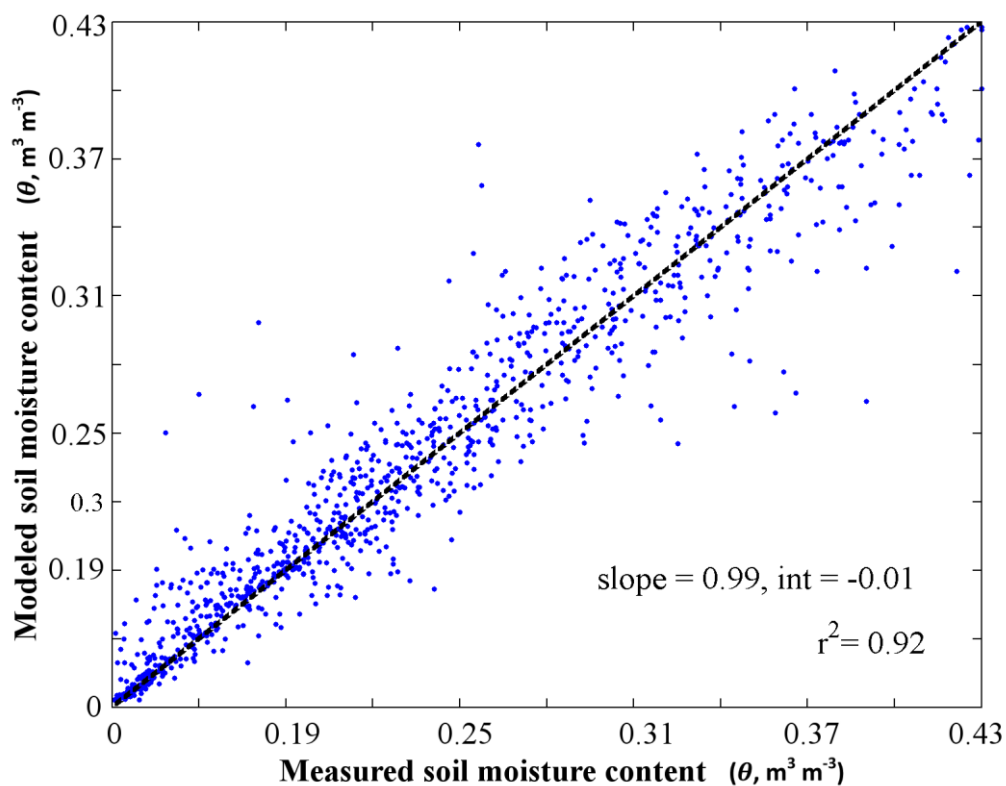433 *moisture content (θ) for the eight site-years of data available from the Duke Pine Forest Site (US-DK3).*

434
435 *Figure S11: The 1:1 comparison between modeled and measured daily soil moisture content in the Duke*
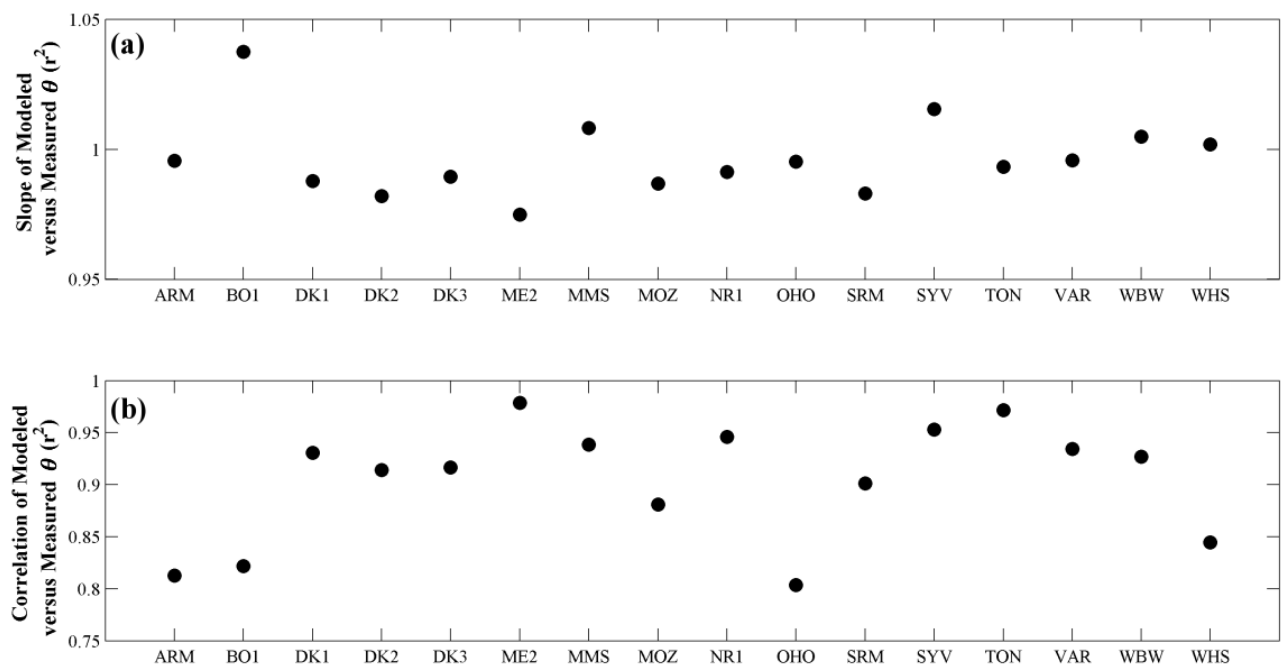436 *Forest Pine Site (US-DK 3).*
437
438
439
440
441

Figure S12: The slope (top panel) and correlation coefficient (bottom panel) between modeled and measured soil moisture content across all of the sites included in the analysis of future limitations to surface conductance and ET.

Future changes in key meteorological drivers: The following figures (Figure S13-16) show the present and projected future means for the key drivers of the Penman-Monteith equation. In every site, nearly all models project increases in future VPD relative to present, occurring concurrently with projected increases in air temperature (T_a). Projected changes in net radiation (R_n) and wind speed (U) are relatively small. Models tend to agree on the change in θ at each site, although across sites no clear trends emerged (i.e., it increases in some, but decreases in others).

Because it is important to preserve the coupling between precipitation and VPD when determining how soil moisture and VPD limit ET, the models were not ensemble averaged. Rather, each of the ten models was used to quantify the limitation to future ET from soil moisture and VPD, and these limitations were then ensemble averaged across the model runs.

458
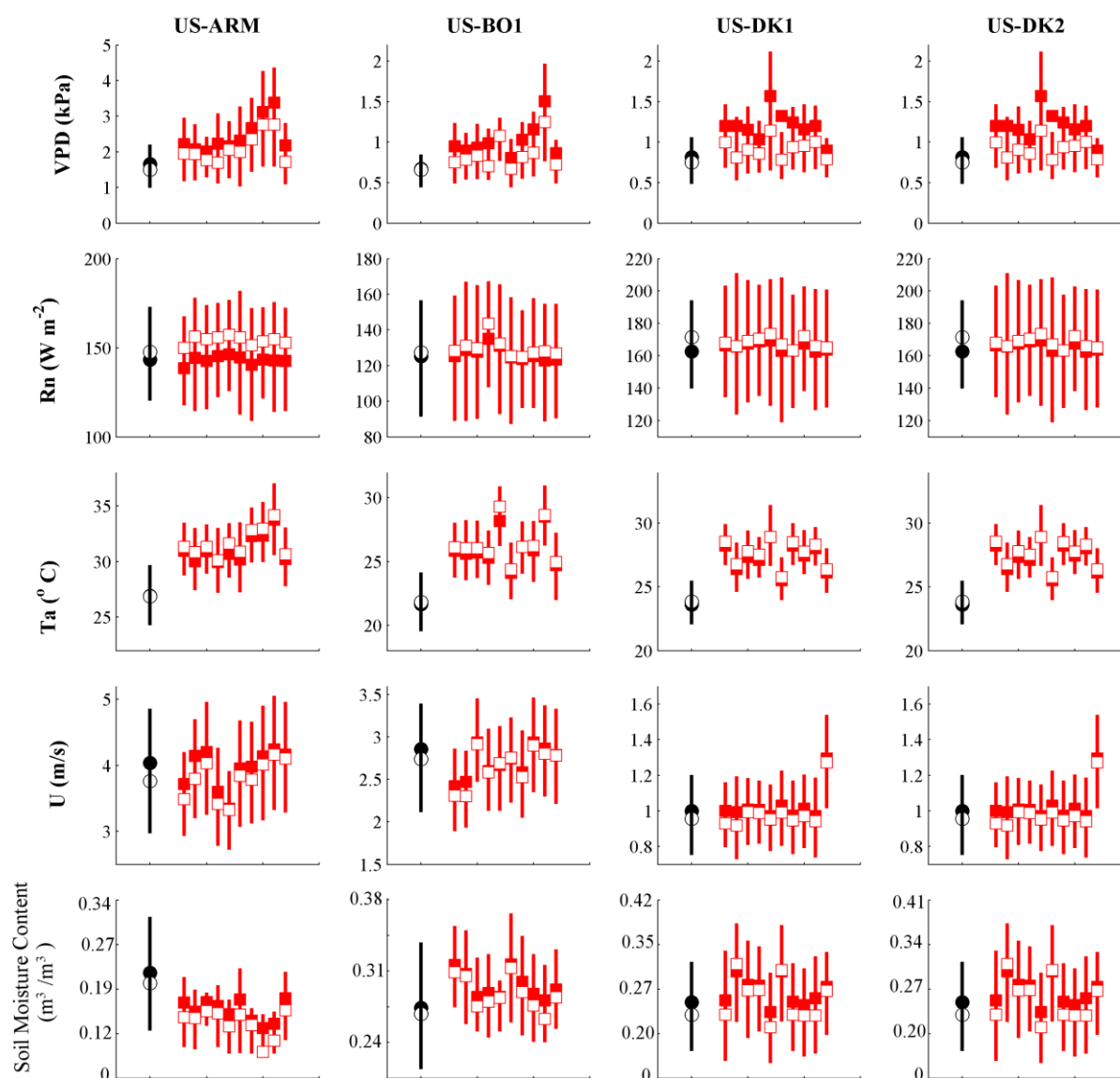
Figure S13: The mean (filled symbols) and median (open symbols) daytime growing season value for key meteorological drivers for present climate conditions (black symbols, derived from Ameriflux observations) and the future (red symbols, derived from model predictions) for select study sites. Error bars show the 50% range daytime values of each variable, and are expected to overlap as these meteorological drivers experience wide shifts over the course of a day and the course of the growing season. The future data and associated error lines are associated with the ten models of Table S3, in sequential order.

466
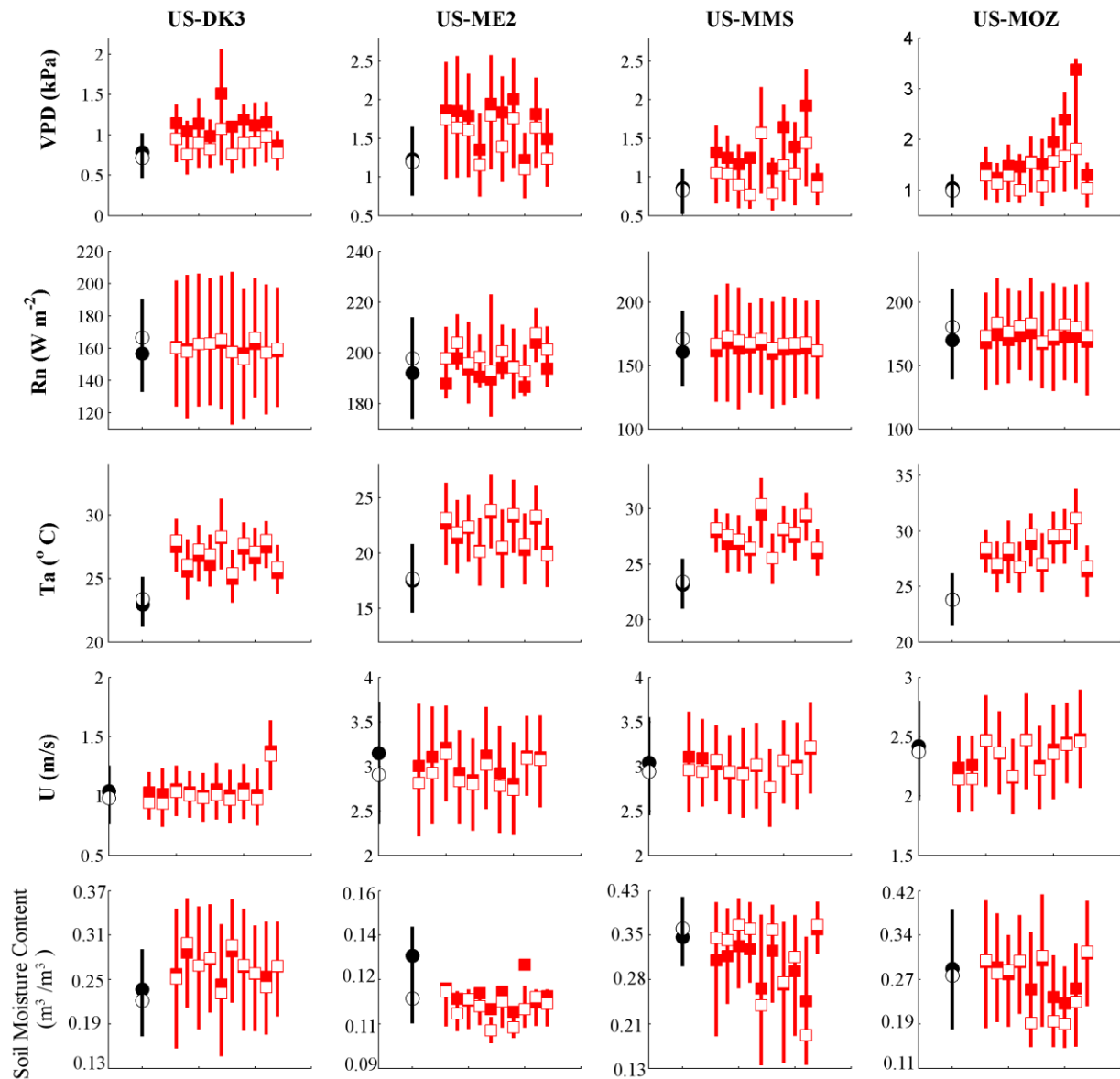
467   *Figure S14: Same as Figure S13, but for additional sites*
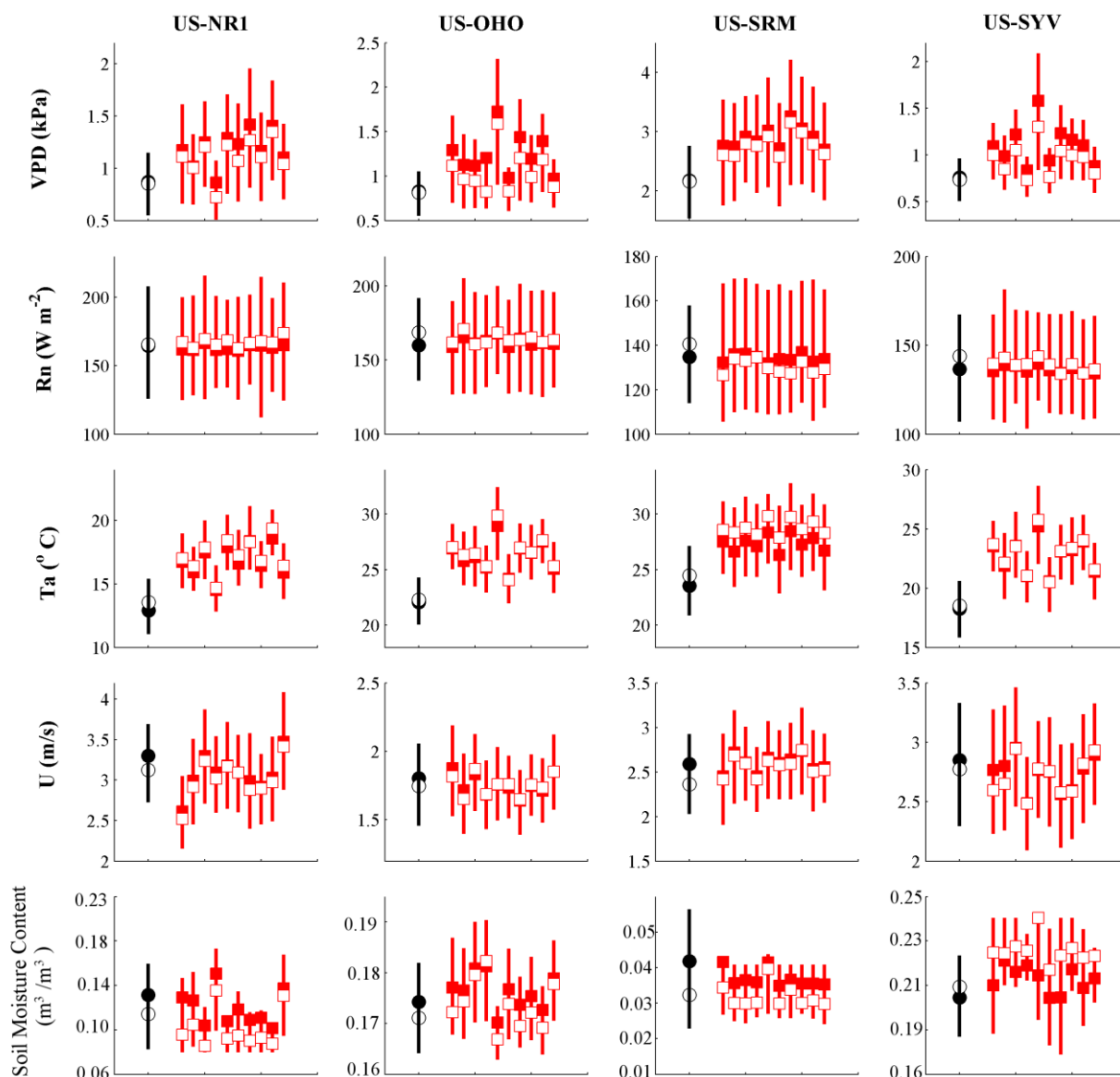
468

469

470

471

472

473

474

475

476   *Figure S15: Same as Figure 14, but for additional sites*

477

478

479

480

481

482

483

484

485
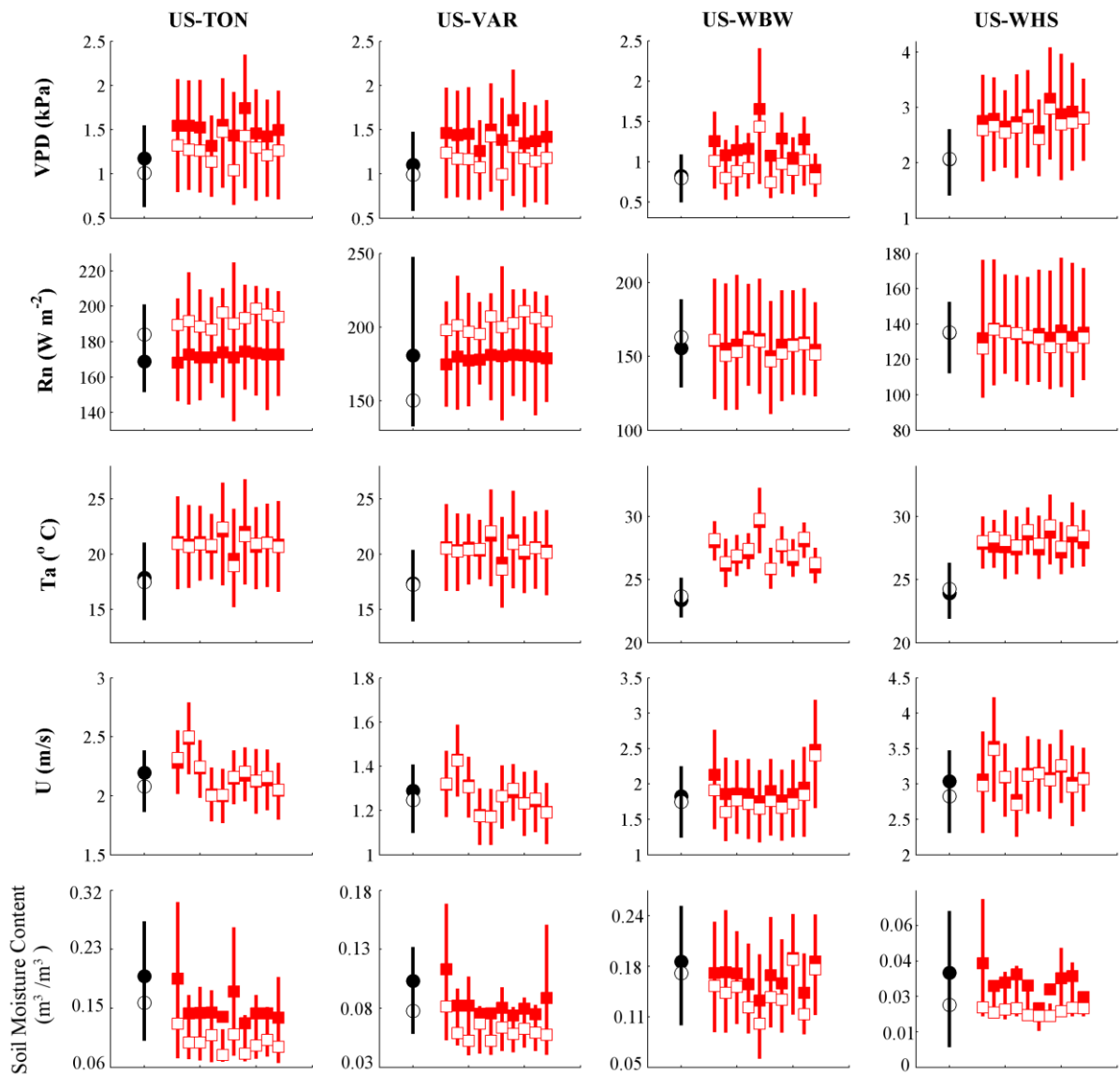
Figure S16: Same as Figure 15, but for additional sites

488

489

490

491 .

492

493

494

495   **Works Cited in the Supplementary Information:**

496

497   1.   Fischer ML, Billesbach DP, Berry JA, Riley WJ, Torn MS. Spatiotemporal variations in growing
498   season exchanges of CO_2, H2O, and sensible heat in agricultural fields of the Southern Great
499   Plains. *Earth Interactions* 2007, **11:** DOI: 10.1175/EI231.1.

500

501   2.   Jenkins JP, Richardson AD, Braswell BH, Ollinger SV, Hollinger DY, Smith ML. Refining light-
502   use efficiency calculations for a deciduous forest canopy using simultaneous tower-based carbon
503   flux and radiometric measurements. *Agricultural and Forest Meteorology* 2007, **143**(1-2): 64-79.

504

505   3.   Goldstein A, Hultman N, Fracheboud J, Bauer M, Panek J, Xu M*, et al.* Effects of climate
506   variability on the carbon dioxide, water, and sensible heat fluxes above a ponderosa pine
507   plantation in the Sierra Nevada (CA). *Agricultural and Forest Meteorology* 2000, **101**(2): 113-
508   129.

509

510   4.   Meyers TP, Hollinger SE. An assessment of storage terms in the surface energy balance of maize
511   and soybean. *Agricultural and Forest Meteorology* 2004, **125**(1-2): 105-115.

512

513   5.   Hernandez-Ramirez G, Hatfield JL, Parkin TB, Sauer TJ, Prueger JH. Carbon dioxide fluxes in
514   corn-soybean rotation in the midwestern US: Inter- and intra-annual variations, and biophysical
515   controls. *Agricultural and Forest Meteorology* 2011, **151**(12): 1831-1842.

516

517   6.   Novick KA, Oishi AC, Ward EJ, Siqueira MBS, Juang JY, Stoy PC. On the difference in the net
518   ecosystem exchange of CO_2 between deciduous and evergreen forests in the southeastern U.S.
519   *Global Change Biology* 2015, **21:** 827-842. .

520

521   7.   Stoy PC, Katul GG, Siqueira MBS, Juang JY, Novick KA, McCarthy HR*, et al.* Role of
522   vegetation in determining carbon sequestration along ecological succession in the southeastern
523   United States. *Global Change Biology* 2008, **14**(6): 1409-1427.

524

525   8.   Allison VJ, Miller RM, Jastrow JD, Matamala R, Zak DR. Changes in soil microbial community
526   structure in a tallgrass prairie chronosequence. *Soil Science Society of America Journal* 2005,
527   **69**(5): 1412-1421.

528

529   9.   Dore S, Kolb TE, Montes-Helu M, Eckert SE, Sullivan BW, Hungate BA*, et al.* Carbon and
530   water fluxes from ponderosa pine forests disturbed by wildfire and thinning. *Ecological
531   Applications* 2010, **20**(3): 663-683.

532

533   10.   Heinsch F, Heilman J, McInnes K, Cobos D, Zuberer D, Roelke D. Carbon dioxide exchange in a
534   high marsh on the Texas Gulf Coast: effects of freshwater availability. *Agricultural and Forest*
535   *Meteorology* 2004, **125**(1)**:** 159-172.

537   11.   Musselman R, Massman W, Frank J, Korfmacher J. The temporal dynamics of carbon dioxide
538   under snow in a high elevation Rocky Mountain subalpine forest and meadow. *Arctic, antarctic,*
539   *and alpine research* 2005, **37**(4)**:** 527-538.

541   12.   Brunsell N, Nippert J, Buck T. Impacts of seasonality and surface heterogeneity on water-use
542   efficiency in mesic grasslands. *Ecohydrology* 2014, **7**(4)**:** 1223-1233.

544   13.   Scott, R.L., Biederman, J.A., Hamerlynck, E.P. and Barron-Gafford, G.A. 2015. The carbon
545   balance pivot point of southwestern U.S. semiarid ecosystems: Insights from the 21st century
546   drought. *Journal of Geophysical Research: Biogeosciences*, 120, 2612-2624. doi:
547   10.1002/2015JG003181.

549   14.   Thomas CK, Martin JG, Law BE, Davis K. Toward biologically meaningful net carbon exchange
550   estimates for tall, dense canopies: Multi-level eddy covariance observations and canopy coupling
551   regimes in a mature Douglas-fir forest in Oregon. *Agricultural and Forest Meteorology* 2013,
552   **173:** 14-27.

554   15.   Verma SB, Dobermann A, Cassman KG, Walters DT, Knops JM, Arkebauer TJ*, et al.* Annual
555   carbon dioxide exchange in irrigated and rainfed maize-based agroecosystems. *Agricultural and*
556   *Forest Meteorology* 2005, **131**(1)**:** 77-96.

558   16.   Campbell J, Sun O, Law B. Supply-side controls on soil respiration among Oregon forests.
559   *Global Change Biology* 2004, **10**(11)**:** 1857-1869.

561   17.   Vickers D, Thomas C, Law BE. Random and systematic CO 2 flux sampling errors for tower
562   measurements over forests in the convective boundary layer. *Agricultural and Forest*
563   *Meteorology* 2009, **149**(1)**:** 73-83.

565   18.   Gu L, Pallardy S, Hosman K, Sun Y. Drought-influenced mortality of tree species with different
566   predawn leaf water dynamics in a decade-long study of a central US forest. *Biogeosciences* 2015,
567   **12**(10)**:** 2831-2845.

569   19.   Seco R, Karl T, Guenther A, Hosman KP, Pallardy SG, Gu L*, et al.* Ecosystem-scale VOC fluxes
570   during an extreme drought in a broad-leaf temperate forest of the Missouri Ozarks (central USA).
571   *Global Change Biology* 2015, **21:** 3657–3674 .

573   20.   Roman DT, Novick KA, Brzostek ER, Dragoni D, Rahman AF, Phillipps R. The role of isohydric
574   and anisohydric species in determining ecosystem-scale response to severe drought. *Oecologia*
575   2015, **179**(3)**:** 641-654.

576

577 21. Noomets A, Gavazzi MJ, McNulty SG, Domec J-C, Sun G, King JS, *et al.* Response of carbon
578   fluxes to drought in a coastal plain loblolly pine forest. *Global Change Biology* 2009, **16**: 272-
579   287.

580 22. Monson R, Turnipseed A, Sparks J, Harley P, Scott-Denton L, Sparks K, *et al.* Carbon
581   sequestration in a high-elevation, subalpine forest. *Global Change Biology* 2002, **8**(5)**:** 459-478.

582

583 23. DeForest JL, Noormets A, McNulty SG, Sun G, Tenney G, Chen J. Phenophases alter the soil
584   respiration–temperature relationship in an oak-dominated forest. *International Journal of
585   Biometeorology* 2006, **51**(2)**:** 135-144.

586

587 24. Sanchez-Mejia ZM, Papuga SA. Observations of a two-layer soil moisture influence on surface
588   energy dynamics and planetary boundary layer characteristics in a semiarid shrubland. *Water
589   Resources Research* 2014, **50**(1)**:** 306-317.

590

591 25. Desai AR, Bolstad PV, Cook BD, Davis KJ, Carey EV. Comparing net ecosystem exchange of
592   carbon dioxide between an old-growth and mature forest in the upper Midwest, USA.
593   *Agricultural and Forest Meteorology* 2005, **128**(1-2)**:** 33-55.

594

595 26. Ma S, Baldocchi DD, Xu L, Hehn T. Inter-annual variability in carbon dioxide exchange of an
596   oak/grass savanna and open grassland in California. *Agricultural and Forest Meteorology* 2007,
597   **147**(3)**:** 157-171.

598

599 27. Curtis PS, Hanson PJ, Bolstad P, Barford C, Randolph J, Schmid H, *et al.* Biometric and eddy-
600   covariance based estimates of annual carbon storage in five eastern North American deciduous
601   forests. *Agricultural and Forest Meteorology* 2002, **113**(1)**:** 3-19.

602

603 28. Verma SB, Baldocchi DD, Anderson DE, Matt DR, Clement RJ. Eddy fluxes of CO_2, water
604   vapor, and sensible heat over a deciduous forest. *Boundary-Layer Meteorology* 1986, **36**(1-2)**:**
605   71-91.

606 29. McDowell N, Barnard H, Bond BJ, Hinckley T, Hubbard RM, Ishii H, *et al.* The relationship
607   between tree height and leaf area: sapwood area ratio. *Oecologia* 2002, **132**(1)**:** 12-20.

608

609 30. Novick K, Oren R, Stoy P, Juang JY, Siqueira M, Katul G. The relationship between reference
610   canopy conductance and simplified hydraulic architecture. *Advances in Water Resources* 2009,
611   **32**(6)**:** 809-819.

612

613 31. Oren R, Sperry JS, Katul GG, Pataki DE, Ewers BE, Phillips N, *et al.* Survey and synthesis of
614   intra- and interspecific variation in stomatal sensitivity to vapour pressure deficit. *Plant Cell
615   Environ* 1999, **22**(12)**:** 1515-1526.

616

617   32.   Williams CA, Reichstein M, Buchmann N, Baldocchi D, Beer C, Schwalm C, *et al*. Climate and
618   vegetation controls on the surface water balance: Synthesis of evapotranspiration measured across
619   a global network of flux towers. *Water Resources Research* 2012, **48**(6).

621   33.   Penman HL. Natural Evaporation from Open Water, Bare Soil and Grass. *Proceedings of the*
622   *Royal Society of London Series a-Mathematical and Physical Sciences* 1948, **193**(1032)**:** 120-&.

624   34.   Monteith JL. Evaporation and environment. In: Fogg BD (ed). *The State and Movement of water*
625   *in Living Organisms, Symposium of the Society of Experimental Biology*, vol. 19. Cambridge
626   University Press: Cambridge, 1965, pp 205-234.

628   35.   Yan H, Wang S, Billesbach D, Oechel W, Zhang J, Meyers T, *et al*. Global estimation of
629   evapotranspiration using a leaf area index-based surface energy and water balance model. *Remote*
630   *sensing of environment* 2012, **124:** 581-595.

632   36.   Wilson KB, Hanson PJ, Mulholland PJ, Baldocchi DD, Wullschleger SD. A comparison of
633   methods for determining forest evapotranspiration and its components: sap-flow, soil water
634   budget, eddy covariance and catchment water balance. *Agricultural and Forest Meteorology*
635   2001, **106**(2)**:** 153-168.

637   37.   Scanlon TM, Kustas WP. Partitioning evapotranspiration using an eddy covariance-based
638   technique: Improved assessment of soil moisture and land–atmosphere exchange dynamics.
639   *Vadose Zone Journal* 2012, **11**(3).

641   38.   Wang L, Niu S, Good SP, Soderberg K, McCabe MF, Sherry RA, *et al*. The effect of warming on
642   grassland evapotranspiration partitioning using laser-based isotope monitoring techniques.
643   *Geochimica Et Cosmochimica Acta* 2013, **111:** 28-38.

645   39.   Oishi AC, Oren R, Novick KA, Palmroth S, Katul GG. Interannual Invariability of Forest
646   Evapotranspiration and Its Consequence to Water Flow Downstream. *Ecosystems* 2010, **13**(3)**:**
647   421-436.

649   40.   Sulman BN, Roman DT, Scanlon TM, Wang L, Novick KA. Comparing methods for partitioning
650   a decade of carbon dioxide and water vapor fluxes in a temperate forest. *Agricultural and Forest*
651   *Meteorology* 2016, **In press**.

653   41.   Baldocchi D, Meyers T. On using eco-physiological, micrometeorological and biogeochemical
654   theory to evaluate carbon dioxide, water vapor and trace gas fluxes over vegetation: a perspective.
655   *Agricultural and Forest Meteorology* 1998, **90**(1)**:** 1-25.

657   42.   Schulze E-D, Kelliher FM, Korner C, Lloyd J, Leuning R. Relationships among maximum
658   stomatal conductance, ecosystem surface conductance, carbon assimilation rate, and plant

659 nitrogen nutrition: a global ecology scaling exercise. *Annual Review of Ecology and Systematics*
660 1994**:** 629-660.

661
662 43.   Allen RG, Pereira LS, Raes D, Smith M. Crop evapotranspiration-Guidelines for computing crop
663   water requirements-FAO Irrigation and drainage paper 56. *FAO, Rome* 1998, **300**(9)**:** D05109.

664
665 44.   Kelliher F, Leuning R, Raupach M, Schulze E-D. Maximum conductances for evaporation from
666   global vegetation types. *Agricultural and Forest Meteorology* 1995, **73**(1)**:** 1-16.

667
668 45.   Campbell GS, Norman JM. *An Introduction to Environmental Biophysics*. Springer-Verlag: New
669   York, 1998.

670
671 46.   Stull RB. *An Introduction to Boundary Layer Meteorology*, vol. 13. Springer, 1988.

672
673 47.   Ruehr NK, Martin JG, Law BE. Effects of water availability on carbon and water exchange in a
674   young ponderosa pine forest: Above-and belowground responses. *Agricultural and forest*
675   *meteorology* 2012, **164:** 136-148.

676
677 48.   Breda N, Huc R, Granier A, Dreyer E. Temperate forest trees and stands under severe drought: a
678   review of ecophysiological responses, adaptation processes and long-term consequences. *Annals*
679   *of Forest Science* 2006, **63**(6)**:** 625-644.

680
681 49.   Clapp RB, Hornberger GM. Empirical equations for some hydraulic properties. *Water Resources*
682   *Research* 1978, **14**(4)**:** 601-604.

683
684 50.   Tyree MT, Sperry JS. Vulnerability of xylem to cavitation and embolism. *Annual review of plant*
685   *biology* 1989, **40**(1)**:** 19-36.

686
687 51.   Granier A, Loustau D, Breda N. A generic model of forest canopy conductance dependent on
688   climate, soil water availability and leaf area index. *Annals of Forest Science* 2000, **57**(8)**:** 755-
689   765.

690
691 52.   Ryan MG, Yoder BJ. Hydraulic limits to tree height and tree growth. *Bioscience* 1997, **47**(4)**:**
692   235-242.

693
694 53.   Jarvis PG. Interpretation of Variations in Leaf Water Potential and Stomatal Conductance Found
695   in Canopies in Field. *Philosophical Transactions of the Royal Society of London Series B-*
696   *Biological Sciences* 1976, **273**(927)**:** 593-610.

697
698 54.   Bernacchi CJ, Pimentel C, Long SP. In vivo temperature response functions of parameters
699   required to model RuBP-limited photosynthesis. *Plant Cell Environ* 2003, **26**(9)**:** 1419-1430.

700

701   55.   Oren R, Sperry JS, Ewers BE, Pataki DE, Phillips N, Megonigal JP. Sensitivity of mean canopy
702   stomatal conductance to vapor pressure deficit in a flooded Taxodium distichum L. forest:
703   hydraulic and non-hydraulic effects. *Oecologia* 2001, **126**(1)**:** 21-29.

704

705   56.   Abatzoglou JT, Brown TJ. A comparison of statistical downscaling methods suited for wildfire
706   applications. *International Journal of Climatology* 2012, **32**(5)**:** 772-780.

707

708   57.   Reichstein M, Falge E, Baldocchi D, Papale D, Aubinet M, Berbigier P*, et al.* On the separation
709   of net ecosystem exchange into assimilation and ecosystem respiration: review and improved
710   algorithm. *Global Change Biology* 2005, **11**(9)**:** 1424-1439.

711

712

713

714